


RESEARCH ARTICLE

Reinforcement learning-adaptive fault-tolerant IGC method for a class of aircraft with non-affine characteristics and multiple uncertainties

Z. Wang^{1,2,3,4}, Y. T. Hao⁴ , J. L. Liu⁴, Y. F. Bai⁵ and D. X. Yu⁶

¹Research Center for Unmanned System Strategy Development, Northwestern Polytechnical University, Xi'an, Shaanxi, China

²National Key Laboratory of Aerospace Flight Dynamics, Northwestern Polytechnical University, Xi'an, Shaanxi, China

³Northwest Institute of Mechanical and Electrical Engineering, Xianyang, China

⁴Unmanned System Research Institute, Northwestern Polytechnical University, Xi'an, Shaanxi, China

⁵China Academy of Launch Vehicle Technology, Beijing, China

⁶School of Artificial Intelligence, Optics and ElectroNics (iOPEN), Northwestern Polytechnical University, Xi'an, Shaanxi, China

Corresponding author: Y. T. Hao; Email: yuting_hao10@163.com

Received: 28 March 2024; **Revised:** 8 July 2024; **Accepted:** 9 July 2024

Keywords: Non-affine integrated guidance and control; Multiple uncertainties; Actor-critic; Adaptive fault-tolerant control

Abstract

In this paper, a brand-new adaptive fault-tolerant non-affine integrated guidance and control method based on reinforcement learning is proposed for a class of skid-to-turn (STT) missile. Firstly, considering the non-affine characteristics of the missile, a new non-affine integrated guidance and control (NAIGC) design model is constructed. For the NAIGC system, an adaptive expansion integral system is introduced to address the issue of challenging control brought on by the non-affine form of the control signal. Subsequently, the hyperbolic tangent function and adaptive boundary estimation are utilised to lessen the jitter due to disturbances in the control system and the deviation caused by actuator failures while taking into account the uncertainty in the NAIGC system. Importantly, actor-critic is introduced into the control framework, where the actor network aims to deal with the multiple uncertainties of the subsystem and generate the control input based on the critic results. Eventually, not only is the stability of the NAIGC closed-loop system demonstrated using Lyapunov theory, but also the validity and superiority of the method are verified by numerical simulations.

Nomenclature

LOS	line of sight
V	velocity
q	pitch rate
n_L	normal accelerationl reference length
S	reference area
m	mass of the missile
I_{yy}	moment of inertia around the pitch axis
T_α	turning rate time constantr range along the LOS
V_r	projections of relative velocities along to the LOS
V_λ	projections of relative velocities orthogonal to the LOS
A_{Tr}	projections of target acceleration along LOS
$A_{T\lambda}$	projections of target acceleration orthogonal to LOS
x_M	x-coordinate of the missile
y_M	y-coordinate of the missile
z_M	z-coordinate of the missile

x_T	x-coordinate of the target
y_T	y-coordinate of the target
z_T	z-coordinate of the target
STT	skid-to-turn
IGC	integrated guidance and control
FTIGC	fault-tolerant integrated guidance and control
NAIGC	non-affine integrated guidance and control
FTC	fault-tolerant control
RL	Reinforcement learning
RBFNN	radial basis function neural network
BS-FTNAIGC	backstepping fault-tolerant non-affine integrated guidance and control
ABE-FTNAIGC	adaptive boundary estimation fault-tolerant non-affine integrated guidance and control
RBF-FTNAIGC	radial basis function fault-tolerant non-affine integrated guidance and control

Greek symbol

α	angle-of-attack
θ	pitch angle
γ_M	track angle
ρ	the density of air
λ	the LOS angle

1.0 Introduction

The integrated guidance and control (IGC) design method has gained significant attention since its initial proposal due to its ability to maximise the missile's flight performance [1] and overall operational effectiveness. By leveraging the coupling relationship between the guidance and control systems, it combines the advantages of low design cost and robustness. Numerous research studies have been dedicated to exploring this method by scholars. Several approaches have been studied for the design of integrated guidance and control, including sliding mode control for designing sliding surfaces [2], optimal control methods [3], feedback linearisation [4], backstepping control method [5], adaptive control [6], and active disturbance rejection control [7]. During the flight of the missile, various failures, such as rudder surface failures, sensor failures, and other mechanical failures, are commonly encountered in the missile systems. Recent research works have focused on fault-tolerant control (FTC) challenges [8–10]. For instance, an adaptive barrier fast terminal sliding mode control method was proposed to mitigate actuator failures in unmanned aerial vehicles [11]. In multi-intelligent systems with node failures and switching topologies, a distributed adaptive fuzzy fault-tolerant control method has been suggested [12]. While there are few FTC-related studies in IGC systems, one literature review has addressed elevator and rudder section failures within strict feedback IGC structures [10]. Asghar et al. [13] considered a burned or broken tailplane failure and developed an IGC system for a ground-to-air missile. Zhao [14] proposed a fault-tolerant control method for handling rudder surface effectiveness loss failures in the vehicle.

Overall, the fault-tolerant integrated guidance and control (FTIGC) design method has attracted extensive research efforts, and various approaches have been explored for the integrated guidance and control system design. Nevertheless, the fault-tolerant controls discussed above are based on the transformation of the vehicle model into an affine input form. The cases where each order of subsystem input to the system is fully non-affine is not considered. In reality, the system is more realistically represented by a non-affine projection. In addition, there is currently no fault-tolerant control design for the non-affine form of the IGC model, with only the literature [15] considering non-affine aerodynamic characteristics to build the IGC model of the STT missile. Undoubtedly, in practical engineering applications,

many parameters of the missile flight and guidance system, such as torque, exhibit non-affine characteristics. Therefore, in this paper, we aim to address the aforementioned problem by developing a new NAIGC scheme for missiles that experience rapidly changing actuator failures and multiple uncertainties from different sources. We describe the missile dynamics and interceptor target kinematics as a non-affine non-linear IGC system, which is more consistent with practical engineering applications.

Reinforcement learning (RL) has gained significant attention as a learning control method due to its ability to deal with unknown uncertainties and has been extensively researched in recent years [16–20]. In Ref. [21], RL was introduced to address the distributed leader-follower output synchronisation problem for linear heterogeneous systems with activities. Moreover, actor-critic structures are frequently employed in reinforcement learning for uncertain systems [22, 23]. The critic network receives information about the system from the task environment and gives a cost function to evaluate the control performance. Based on the cost function, the actor network is used to generate the next control policy for the actuator. Ouyang et al. [24] designed an actor-critic adaptive control method for tracking control of an uncertain elastic joint robot. The critical neural network was used to approximate the cost function, while the actor neural network was used to handle system uncertainty and generate control inputs for the actuator. Liu et al. [25] proposed an incremental reinforcement learning control method with adaptive learning rate to improve the success rate of flight controllers. A distributed reinforcement learning guidance strategy under angle-of-attack constraints was investigated in Ref. [26]. Pei et al. [27] used the deep deterministic policy gradient algorithm to integrate guidance control into a reinforcement learning framework to intercept targets using reinforcement learning-generated intelligences, and numerically verified the effectiveness and robustness of the method. In the literature [28], the IGC system was modeled as a reinforcement learning process based on a three degrees of freedom motion model of the hypersonic vehicles in the longitudinal plane, and a proximal policy optimisation algorithm-based IGC system was designed. It can be seen that the performance of reinforcement learning actor-critic is satisfactory for controlling the vehicle or guidance system. The model of the IGC problem exhibits intricate nonlinear dynamics, encompassing non-linear relationships, non-affine terms and uncertain disturbances. Simultaneously, the IGC problem necessitates a high level of certainty in the control scheme, demanding precise system control in accordance with predetermined planning trajectories. The reinforcement learning actor-critic approach has yet to be investigated for its applicability when dealing with such complex models.

The sensor measurement bias, as well as the actuator effectiveness failure and bias failure generated during the flight, can disturb the attitude control system, which makes the controller design more challenging. In addition, external disturbances and structural uncertainties should be considered, which can also cause troubles during the controller design process. Inspired by the above, this paper will focus on the FTIGC problem for a class of non-affine forms with structural uncertainties, actuator failures and external disturbances in the NAIGC system. The main challenges of this paper are how to model the NAIGC system and how to deal with the non-affine problem and various unknown uncertainties and time-varying fault variations. By introducing an adaptive expansion integral system to deal with the non-simulation problem and fully combining the reinforcement learning actor-critic architecture and the approximation capability of radial basis function neural network (RBFNN), the unknown uncertainties and fault problems can be well handled by using bounded adaptive control techniques. Compared with existing results, the method proposed in this paper has the following contributions:

- To the best of the authors' knowledge, the method applying actor-critic to the design of adaptive fault-tolerant NAIGC is proposed for the first time and can be an effective solution of solving multiple uncertainties.
- A new type of non-affine integrated guidance and control design model is established for a class of STT missile with actuator failures and multiple uncertainties and can be extended to other aircraft with non-affine structures.

- Benefiting from the combination of adaptive boundary, RBFNN, and actor-critic, the missile’s ability to respond to actuator failures and formulation and preliminaries of target manoeuvres problem can be greatly improved.

2.0 Problem formulation and preliminaries

2.1 Non-affine IGC model

Consider the following nonlinear longitudinal model of the missile where the gravity and the coupling between the longitudinal and lateral channel are neglected:

$$\begin{aligned}
 \dot{\alpha} &= q + \frac{-0.5\rho V^2 S c_{x'}(\alpha) \sin \alpha + 0.5\rho V^2 S (c_{z1}(\alpha) + c_{z2}(\alpha)M_m) \cos \alpha}{mV} \\
 \dot{V} &= \frac{0.5\rho V^2 S c_{x'}(\alpha) \cos \alpha + 0.5\rho V^2 S (c_{z1}(\alpha) + c_{z2}(\alpha)M_m) \sin \alpha}{m} \\
 \dot{q} &= \frac{0.5\rho V^2 S l (c_{m1}(\alpha) + c_{m2}(\alpha)M_m + c_m^{\delta_e} \delta_e)}{I_{yy}} \\
 \dot{\theta} &= q \\
 \dot{n}_L &= \frac{-n_L + Vq}{T_\alpha} \\
 \gamma_M &= \theta - \alpha
 \end{aligned} \tag{1}$$

where $c_x, c_{z1}, c_{z2}, c_{m1}, c_{m2}, c_m^{\delta_e}$ denote the aerodynamic coefficients.

The kinematics of a planar missile intercept target can be described as [29]:

$$\begin{aligned}
 \dot{r} &= V_r \\
 \dot{V}_r &= \frac{V_\lambda^2}{r} + A_{Tr} - \sin(\lambda - \gamma_M) n_L \\
 \dot{\lambda} &= \frac{V_\lambda}{r} \\
 \dot{V}_\lambda &= -\frac{V_\lambda V_r}{r} + A_{T\lambda} - \cos(\lambda - \gamma_M) n_L
 \end{aligned} \tag{2}$$

Considering the actuator fault, $u(t)$ is defined as the actuator inputs. Then the output of the actuator fault is expressed as

$$\delta_e = \lambda_\delta(t) u(t) + d_\delta(t) \tag{3}$$

where d_δ represents the error of the actuator malfunction. λ_δ represents the scale factor of the actuator gain fault. Assume that d_δ is a bounded unknown variable, λ_δ takes values in the interval [0,1]. According to the corollary of Ref. [10], when $V_\lambda \rightarrow k_0\sqrt{r}$, where $k_0 > 0$ is a constant, the direct hit can be obtained. Thus by defining $\chi = V_\lambda - k_0\sqrt{r}$, we can obtain the time derivative of χ .

$$\dot{\chi} = -\frac{V_\lambda V_r}{r} + A_{T\lambda} - \cos(\lambda - \gamma_M) n_L - \frac{k_0 V_r}{2\sqrt{r}} \tag{4}$$

Meanwhile, according to the kinetic eqnarrays of n_L and q , we can obtain

$$\begin{aligned}
 \dot{n}_L &= -\frac{n_L}{T_\alpha} + \frac{V}{T_\alpha} q \\
 \dot{q} &= \frac{\rho V^2 S l (c_{m1}(\alpha) + c_{m2}(\alpha)M_m)}{2I_{yy}} + \frac{\rho V^2 S l c_m^{\delta_e}}{2I_{yy}} \delta_e
 \end{aligned} \tag{5}$$

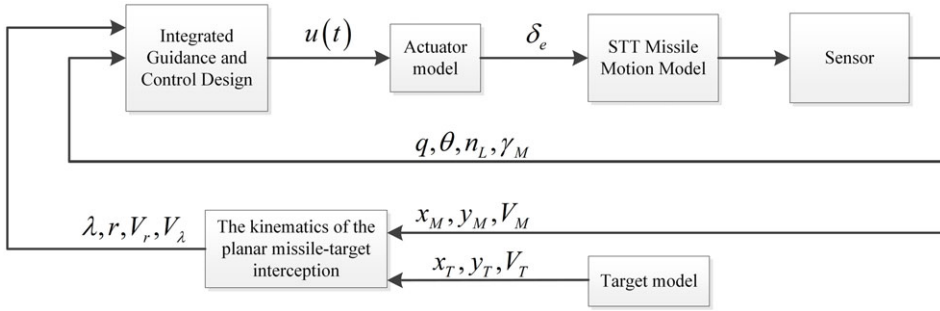


Figure 1. The relationship between the outer and inner loops of the guidance and control integration.

Define $x_1 = \chi, x_2 = n_L, x_3 = q$ and

$$\begin{aligned}
 f_1 &= -\frac{V_\lambda V_r}{r} - \frac{k_0 V_r}{2\sqrt{r}}, g_1 = \cos(\lambda - \gamma_M) (1 + \Delta b_1) x_2, d_1 = A_{T\lambda} \\
 f_2 &= \frac{-n_L}{T_\alpha}, g_2 = \frac{V}{T_\alpha} (1 + \Delta b_2) x_3, d_3 = \frac{\rho V^2 S l c_m^{\delta_e}}{2I_{yy}} (1 + \Delta b_3) d_\delta \\
 f_3 &= \frac{\rho V^2 S l (c_{m1}(\alpha) + c_{m2}(\alpha) M_m)}{2I_{yy}}, g_3 = \frac{\rho V^2 S l c_m^{\delta_e}}{2I_{yy}} (1 + \Delta b_3) \lambda_3 u
 \end{aligned} \tag{6}$$

We can get the following non-affine system,

$$\begin{aligned}
 \dot{x}_1 &= f_1(t, x_1) + g_1(t, x_1, x_2) + d_1(t) + \Delta f_1(t, x_1) \\
 \dot{x}_2 &= f_2(t, x_1, x_2) + g_2(t, x_1, x_2, x_3) + \Delta f_2(t, x_1, x_2) \\
 \dot{x}_3 &= f_3(t, x_1, x_2, x_3) + g_3(t, x_1, x_2, x_3, u) + d_3(t) + \Delta f_3(t, x_1, x_2, x_3) \\
 y &= x_1
 \end{aligned} \tag{7}$$

where $x_i \in R^i, i = 1, 2, 3$ are system state variables. $y = x_1$ is the system output. Δf_i and $\Delta b_i, i = 1, 2, 3$ are the uncertainty caused by the measurement error, in fact, $\Delta b_i \in [-0.5, +0.5]$. Obviously the integrated design model of guidance control is a third-order non-affine system, and the relationship between the outer and inner loops is shown schematically in Fig. 1.

Remark 1. The non-affine IGC model established in this paper is more general, and the aerodynamic characteristics of the missile and the rate of change of deflection are considered in the form of non-affine functions, so that each subsystem contains non-affine inputs, which has great reference significance for practical engineering applications, but also makes the design of the controller more difficult.

The design goal of this paper is to design a class of RBFNN and actor-critic based adaptive controllers such that the control converges to zero in the presence of multiple factors such as actuator failure, simultaneous changes in unknown target acceleration, and coupled multi-source uncertainty, and that the relevant gain parameters in the controllers converge with bounds.

In this article, the following assumptions are necessary:

Lemma 1. [30] The following inequality holds for any $\varepsilon > 0$ and $z \in R$, we have

$$0 \leq |z| - z \tanh\left(\frac{z}{\varepsilon}\right) \leq \kappa \varepsilon \tag{8}$$

where κ is a positive number satisfying $\kappa = e^{-(\kappa+1)}$, i.e., $\kappa = 0.2785$

Lemma 2. [31] (Cauchy inequality) $\|\bullet\|$ is the Euclidean paradigm of the vector, i.e. $\|x\| = \sqrt{x^T x}$. For $\forall x, y \in R^m$, the following inequality holds:

$$\|x^T y\| \leq \|x\| \|y\| \tag{9}$$

Lemma 3. [32] (Young inequality) Given normal numbers p and q that satisfy $1/p + 1/q = 1$, to any $x, y \in$ and any $\varepsilon > 0$, the following inequality is true:

$$|xy| \leq \frac{\varepsilon^p}{p} |x|^p + \frac{1}{q\varepsilon^q} |y|^q \tag{10}$$

Lemma 4. [33] The Lyapunov function $V(t)$ with initial bounded condition $V(0)$, if the derivative of $V(t)$ satisfies

$$\dot{V}(t) \leq -C_V V(t) + E_V \tag{11}$$

where C_V and E_V are positive constants, $V(t)$ is bounded.

Lemma 5. [34] For any constant $\varepsilon > 0$ and any variable $z \in R$, the following relationship holds

$$|z| < \frac{z^2}{\sqrt{z^2 + \varepsilon^2}} + \varepsilon \tag{12}$$

Assumption 1. There exist positive constants \underline{g} and \bar{g} , the following inequality holds

$$\bar{g} \geq \left\| \frac{\partial g_i(\bar{x}_{i+1})}{\partial x_j} \right\| \geq \underline{g}, i = 1, \dots, n. \quad j = 1, \dots, n + 1. \tag{13}$$

where $\bar{x}_{i+1} = [x_1, \dots, x_{i+1}]$, $i = 1, \dots, n$. $x_{n+1} = u$

Remark 2. This assumption is introduced to make the whole system controllable.

2.2 Neural networks for approximation

In this paper, we require to approximate the system uncertainty and unknown cost functions. System uncertainty is estimated using RBFNN, which is a three-layer network. The first layer is called the input layer, the second layer is called the hidden layer. RBFNN generally contains only one hidden layer, and the weights of all neurons from the input to the hidden layer are 1. The third layer is called the output layer. In this paper, we use the following Gaussian function, denoted as $\phi(x)$, as the radial basis function: μ_j is the function centroid of the j -th node of the hidden layer, and σ_j is the width of the j -th node:

$$\phi(x) = \exp\left(-\frac{\|x - \mu_j\|^2}{2\sigma_j^2}\right) \tag{14}$$

The final output is defined as

$$y = \frac{\sum_{j=1}^m w_j \sum_{i=1}^n \exp\left(-\frac{\|x_i - \mu_j\|^2}{2\sigma_j^2}\right)}{\sum_{j=1}^m \sum_{i=1}^n \exp\left(-\frac{\|x_i - \mu_j\|^2}{2\sigma_j^2}\right)} = \hat{W}^T \Phi(x) \tag{15}$$

where $x \in R^n$ and $y \in R$ are the input and output of RBFNN, respectively. $\hat{W} = [w_1, \dots, w_m]^T \in^m$ denotes the output layer weight matrix, m represents the number of hidden nodes in the hidden layer. $\Phi(x) = [\Phi_1(x), \dots, \Phi_m(x)]^T$, where:

$$\Phi_j(x) = \frac{\sum_{i=1}^n \exp\left(-\frac{\|x_i - \mu_j\|^2}{2\sigma_j^2}\right)}{\sum_{j=1}^m \sum_{i=1}^n \exp\left(-\frac{\|x_i - \mu_j\|^2}{2\sigma_j^2}\right)} \tag{16}$$

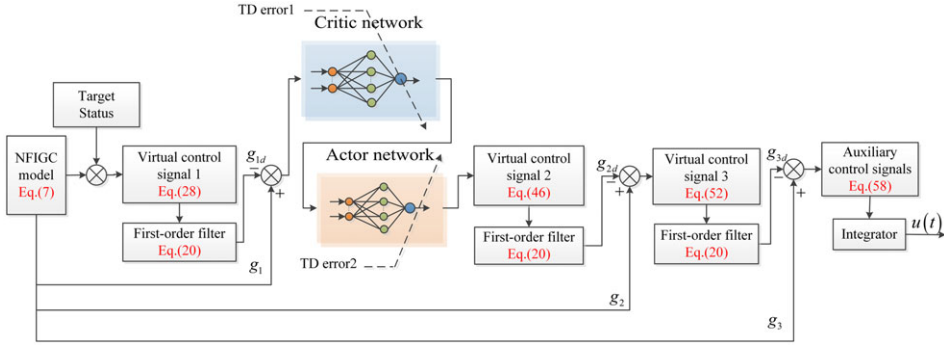


Figure 2. Integrated guidance and control design block diagram.

It has been shown that for the smooth function, there exists an optimal weight [35], such that

$$f(x) = W^T \Phi(x) + \varepsilon(x) \tag{17}$$

where $\varepsilon(x)$ is the approximation error, which can be made arbitrarily small by increasing the number of nodes in the hidden layer.

Assumption 2. For the basic functions used for fitting in the actor-critic neural network mentioned later $\Psi_a(Z_a)$ and $\Psi_J(Z_c)$, they satisfy $\beta_a \leq \|\Psi_a\| \leq \psi_a$, $\beta_J \leq \|\Psi_J\| \leq \psi_J$ and for the derivatives of $\Psi_a(Z_a)$ and $\Psi_J(Z_c)$, they satisfy $\lambda_a \leq \|\dot{\Psi}_a\| \leq \gamma_a$, $\lambda_J \leq \|\dot{\Psi}_J\| \leq \gamma_J$. In addition, the derivatives of the estimation error and the estimation error are bounded when using neural network fitting approximation simultaneously, $|\varepsilon_i(Z)| \leq \varsigma_i$, $|\dot{\varepsilon}_i(Z)| \leq \xi_i$, where ς_i, ξ_i are positive numbers.

3.0 Main results

To solve the problem of non-affine inputs in the system (7), an auxiliary integral system is introduced, and as an auxiliary control input, the augmented system is expressed as

$$\begin{aligned} \dot{x}_1 &= f_1(t, x_1) + g_1(t, x_1, x_2) + d_1(t) + \Delta f_1 \\ \dot{x}_2 &= f_2(t, x_1, x_2) + g_2(t, x_1, x_2, x_3) + \Delta f_2 \\ \dot{x}_3 &= f_3(t, x_1, x_2, x_3) + g_3(t, x_1, x_2, x_3, u) + d_3(t) + \Delta f_3 \\ \dot{u} &= u_f \end{aligned} \tag{18}$$

Remark 3. By adding an auxiliary integration system, the original third-order non-affine input system is transformed into a fourth-order affine input system, which effectively overcomes the non-affine input problem in the system (7).

The backpropagation design process, influenced by the non-affine input, consists of four steps, and the actual control is given in Step 4, and the control box is shown in Fig. 2.

3.1 Design steps of the reinforcement learning adaptive fault-tolerant IGC method

Define the error variables as follows

$$\begin{aligned} z_1(t) &= x_1(t) \\ z_2(t) &= g_1(t) - g_{1d} \\ z_3(t) &= g_2(t) - g_{2d} \\ z_4(t) &= g_3(t) - g_{3d} \end{aligned} \tag{19}$$

where $g_{id}, i = 1, 2, 3$ is the filtered signal of the virtual control law for the i -th subsystem. We introduce a new variable g_{ic} obtained from

$$\tau_i \dot{g}_{id} + g_{id} = g_{ic}, g_{id}(0) = g_{ic}(0) \tag{20}$$

Remark 4. By introducing dynamic surfaces, the derivatives of the controllers in the simulation programme can be transformed, which in turn reduces the complexity of the operations.

The boundary layer error is defined as

$$y_i = g_{id} - g_{ic} \tag{21}$$

where g_{ic} is the virtual control law designed for the i -th subsystem. $0 < \tau_i < 1, i = 1, 2, 3$ is the filtering time constant to be designed. Then combining Equations (20) and (21) we can obtain that

$$\dot{y}_i = \dot{g}_{id} - \dot{g}_{ic} = -\frac{y_i}{\tau_i} - \dot{g}_{ic} \tag{22}$$

Furthermore, for the unknown nonlinear function, we define

$$\theta_i = \max \left\{ \sup_{t \geq 0} \|W_i\| : i = 1, 2, 3 \right\} \tag{23}$$

Let $\hat{\theta}$ be the estimations of θ . The corresponding estimation errors are defined as $\tilde{\theta} = \hat{\theta} - \theta$.

3.1.1 Step 1

Define $D_1 = \sup_{t \geq 0} \|d_1(t)\|$. Denote \hat{D}_1 as the estimate of D_1 . Moreover, assuming that the disturbance error $\bar{\varepsilon}_{D_1}$ estimated by the tanh function bounder is bounded:

$$\left| d_1 - \hat{D}_1 \tanh \left(\frac{z_1}{\varepsilon_{D_1}} \right) \right| \leq \bar{\varepsilon}_{D_1} \tag{24}$$

where $\varepsilon_{D_1} > 0$ is a parameter to be designed. Combining Equations (18) and (21) and the first formula of Equation (19), we can get that

$$\dot{z}_1 = \dot{x}_1 = f_1 + z_2 + g_{1c} + y_1 + d_1 + \Delta f_1 \tag{25}$$

Hence, it follows that

$$z_1 \dot{z}_1 = z_1 (f_1 + z_2 + g_{1c} + y_1 + d_1 + \Delta f_1) \tag{26}$$

RBFNN is introduced to approximate the nonlinearity Δf_1 in Equation (18). Obviously $\Delta f_1 = W_1^T \Phi_1(x_1) + \varepsilon_{\Delta_1}(x_1)$, $\varepsilon_{\Delta_1}(x_1)$ is the RBFNN estimation error with an upper bound ε_{m1} .

Based on Lemma 2, Lemma 3 and Lemma 5, we can obtain that

$$\begin{aligned} z_1 \Delta f_1 &= z_1 W_1^T \Phi_1(x_1) + z_1 \varepsilon_{\Delta_1}(x_1) \\ &\leq \|W_1^T\| \|z_1 \Phi_1(x_1)\| + \|z_1\| \varepsilon_{m1} \leq \theta_1 z_1 \bar{\Phi}_{11} + \frac{1}{2} z_1^2 + \frac{1}{2} \varepsilon_{m1}^2 \tag{27} \\ \bar{\Phi}_{11} &= \left(\frac{z_1 \Phi_1^T(x_1) \Phi_1(x_1)}{\sqrt{z_1^2 \Phi_1^T(x_1) \Phi_1(x_1) + \varepsilon_{11}^2}} + \varepsilon_{11} \right) \end{aligned}$$

where $\varepsilon_{11} > 0$ is a parameter to be designed.

Remark 5. In this paper, in order to reduce the computational burden, so the upper bound of the neural network weight parametrisation is used for adaptive compensation, or it can be solved directly with a multi-dimensional vector without the upper bound, and the final controller as well as the form of the adaptive update law are similar to this method.

The virtual controller can be designed as follows

$$g_{1c} = -k_1 z_1 - \hat{\theta}_1 \bar{\Phi}_{11} - \hat{D}_1 \tanh\left(\frac{z_1}{\varepsilon_{D_1}}\right) - f_1 \tag{28}$$

where $k_1 > 0$ is a parameter to be designed.

Combining Equations (26)–(28), we can rewrite Equation (26) as

$$z_1 \dot{z}_1 \leq -k_1 z_1^2 + z_1 (z_2 + y_1) + z_1 \left(d_1 - \hat{D}_1 \tanh\left(\frac{z_1}{\varepsilon_{D_1}}\right) \right) - z_1 \tilde{\theta}_1 \bar{\Phi}_{11} + \frac{1}{2} z_1^2 + \frac{1}{2} \varepsilon_{m1}^2 \tag{29}$$

Define the adaptive update law of \hat{D}_1 is

$$\dot{\hat{D}}_1 = \eta_{D_1} z_1 \tanh\left(\frac{z_1}{\varepsilon_{D_1}}\right) - \eta_{D_1} \sigma_{D_1} \hat{D}_1 \tag{30}$$

where $\eta_{D_1}, \sigma_{D_1} > 0$ are parameters to be designed.

3.1.2 Step 2

We define the cost function as follows

$$J(t) = \int_0^T c(t) dt = \int_0^T (g_1 - g_{1d})^2 dt \tag{31}$$

i.e., $c = \dot{J}$.

Critic network: Due to the non-deterministic nature of the cost function, the neural network can be used to estimate as

$$J(t) = \Theta_J^T \Psi_J(Z_c) + \varepsilon_J \tag{32}$$

where $\Theta_J \in R^{l_c}$ is the ideal critic network weight. l_c represents the number of hidden nodes. ε_J represents the estimation error. $Z_c = [z_2]$ is the input to the critic neural network. Define the estimate of the cost function as

$$\hat{J}(t) = \hat{\Theta}_J^T \Psi_J(Z_c) \tag{33}$$

where $\hat{\Theta}_J$ is the actual critic network weight and we have $\tilde{\Theta}_J = \hat{\Theta}_J - \Theta_J$ with $\tilde{\Theta}_J$ being the critic neural network weight error. Then we define a critic error as

$$\varepsilon_{critic} = c(t) + \hat{\Theta}_J^T \dot{\Psi}_J(Z_c) \tag{34}$$

The function of the critic error can be designed as

$$E_{critic} = \frac{1}{2} \varepsilon_{critic}^2 \tag{35}$$

In the framework of σ -modification, using the gradient descent method, we can obtain the update law of $\hat{\Theta}_J$ as

$$\dot{\hat{\Theta}}_J = -\eta_J \frac{\partial E_{critic}}{\partial \hat{\Theta}_J} = -\eta_J \frac{\partial E_{critic}}{\partial \varepsilon_{critic}} \cdot \frac{\partial \varepsilon_{critic}}{\partial \hat{\Theta}_J} = -\eta_J \varepsilon_{critic} \dot{\Psi}_J(Z_c) - \sigma_J \eta_J \hat{\Theta}_J \tag{36}$$

Actor network: with Equation (18), Equation (21) and the second formula of Equation (19), we can get that

$$\begin{aligned} \dot{z}_2 &= \dot{g}_1 - \dot{g}_{1d} \\ &= \frac{\partial g_1}{\partial x_1} \dot{x}_1 + \frac{\partial g_1}{\partial x_2} \dot{x}_2 - \dot{g}_{1d} \\ &= \frac{\partial g_1}{\partial x_1} (f_1 + g_1 + d_1 + \Delta f_1) + \frac{\partial g_1}{\partial x_2} (f_2 + \Delta f_2 + z_3 + y_2 + g_{2c}) - \dot{g}_{1d} \end{aligned} \tag{37}$$

Thus

$$z_2 \dot{z}_2 = z_2 \left(\frac{\partial g_1}{\partial x_1} (f_1 + d_1 + \Delta f_1) + \frac{\partial g_1}{\partial x_2} (f_2 + z_3 + g_{2c} + y_2 + \Delta f_2) - \dot{x}_{1d} \right) \tag{38}$$

By using Lemmas 2, 3 and 5, we have

$$\begin{aligned} z_2 \Delta f_1 &= z_2 W_1^T \Phi_1(x_1) + z_2 \varepsilon_{\Delta_1}(x_1) \\ &\leq \|W_1^T\| \|z_2 \Phi_1(x_1)\| + \|z_2\| \varepsilon_{m1} \leq \theta_1 z_2 \bar{\Phi}_{12} + \frac{1}{2} z_2^2 + \frac{1}{2} \varepsilon_{m1}^2 \\ \bar{\Phi}_{12} &= \left(\frac{z_2 \Phi_1^T(x_1) \Phi_1(x_1)}{\sqrt{z_2^2 \Phi_1^T(x_1) \Phi_1(x_1) + \varepsilon_{12}^2}} + \varepsilon_{12} \right) \end{aligned} \tag{39}$$

where $\varepsilon_{12} > 0$ is a parameter to be designed. Based on the approximation of the neural network, the uncertainty Δf_2 in Equation (18) is approximated as

$$\Delta f_2(t, x_1, x_2) = \Theta_a^T \Psi_a(Z_a) + \varepsilon_a(Z_a) \tag{40}$$

where $\Theta_a \in R^{l_a}$ is the ideal critic network weight with l_a denoting the number of hidden nodes, $Z_a = [x_1, x_2]^T$ is the input to the actor neural network, and $\varepsilon_a(Z_a)$ denotes the function reconstruction error. Additionally, $\hat{\Theta}_a$ is the actual actor network weight, and $\tilde{\Theta}_a = \hat{\Theta}_a - \Theta_a$, $\tilde{\Theta}_a$ is the actor neural network weight error. Then we design a actor error as

$$\varepsilon_{actor} = \frac{\partial g_1}{\partial x_2} \tilde{\Theta}_a^T \Psi_a(Z_a) + \hat{J} \tag{41}$$

We define the actor error function as

$$E_{actor} = \frac{1}{2} \varepsilon_{actor}^2 \tag{42}$$

According to the gradient descent method, we can get the update law of $\hat{\Theta}_a$ as

$$\dot{\hat{\Theta}}_a = -\eta_a \frac{\partial E_{actor}}{\partial \hat{\Theta}_a} = -\eta_a \frac{\partial E_{actor}}{\partial \varepsilon_{actor}} \cdot \frac{\partial \varepsilon_{actor}}{\partial \hat{\Theta}_a} = -\frac{\partial g_1}{\partial x_2} \eta_a \varepsilon_{actor} \Psi_a(Z_a) \tag{43}$$

However, since $\tilde{\Theta}_a$ is unknown, so that we let $\hat{\Theta}_a$ replace $\tilde{\Theta}_a$. Substituting Equation (41) into Equation (43) yields

$$\dot{\hat{\Theta}}_a = -\frac{\partial_1}{\partial x_2} \eta_a \left(\frac{\partial g_1}{\partial x_2} \hat{\Theta}_a^T \Psi_a(Z_a) + \hat{J} \right) \Psi_a(Z_a) \tag{44}$$

By introducing σ correction, Equation (44) can be rewritten as

$$\dot{\hat{\Theta}}_a = -\frac{\partial g_1}{\partial x_2} \eta_a \left(\frac{\partial g_1}{\partial x_2} \hat{\Theta}_a^T \Psi_a(Z_a) + \hat{J} \right) \Psi_a(Z_a) - \sigma_a \eta_a \hat{\Theta}_a \tag{45}$$

We design the following virtual controller

$$g_{2c} = \frac{1}{\frac{\partial g_1}{\partial x_2}} \left(-k_2 z_2 - \frac{\partial g_1}{\partial x_1} \left(f_1 + g_1 + \hat{D}_1 \tanh \left(\frac{z_1}{\varepsilon_{D1}} \right) + \hat{\theta}_1 \bar{\Phi}_{12} \right) - \frac{\partial g_1}{\partial x_2} \left(\hat{\Theta}_a^T \Psi_a(Z_a) + f_2 \right) - \frac{y_1}{\tau_1} \right) \tag{46}$$

where $k_2 > 0$ is a parameter to be designed. With the aid of Equations (38)–(46) we know that

$$\begin{aligned} z_2 \dot{z}_2 &\leq -k_2 z_2^2 + \frac{\partial g_1}{\partial x_1} z_2 \left(d_1 - \hat{D}_1 \tanh \left(\frac{z_1}{\varepsilon_{D1}} \right) \right) - \frac{\partial g_1}{\partial x_1} z_2 \tilde{\theta}_1 \bar{\Phi}_{12} + \frac{\partial_1}{\partial x_2} (z_3 + y_2) \\ &\quad - \frac{\partial g_1}{\partial x_2} z_2 \tilde{\Theta}_a^T \Psi_a(Z_a) + \frac{\partial g_1}{\partial x_2} z_2 \varepsilon_a(Z_a) + \frac{1}{2} z_2^2 + \frac{1}{2} \varepsilon_{m1}^2 \end{aligned} \tag{47}$$

3.1.3 Step 3

Define $D_3 = \sup_{t \geq 0} \|d_3(t)\|$, \hat{D}_3 is the estimate of D_3 . Furthermore, assuming that the disturbance error $\bar{\varepsilon}_{D_3}$ estimated by the tanh function bounder is bounded

$$\left| d_3(t) - \hat{D}_3 \tanh\left(\frac{\partial g_2}{\partial x_3} \cdot \frac{z_3}{\varepsilon_{D_3}}\right) \right| \leq \bar{\varepsilon}_{D_3} \tag{48}$$

where $\varepsilon_{D_3} > 0$ is a parameter to be designed. In view of Equations (18), (21) and the third formula of Equation (19), we can get that

$$\begin{aligned} \dot{z}_3 &= \dot{g}_2 - \dot{g}_{2d} = \frac{\partial g_2}{\partial x_1} \dot{x}_1 + \frac{\partial g_2}{\partial x_2} \dot{x}_2 + \frac{\partial g_2}{\partial x_3} \dot{x}_3 - \dot{g}_{2d} \\ &= \frac{\partial g_2}{\partial x_1} (f_1 + g_1 + d_1 + \Delta f_1) + \frac{\partial g_2}{\partial x_2} (f_2 + g_2 + \Delta f_2) \\ &\quad + \frac{\partial g_2}{\partial x_3} (f_3 + z_4 + g_{3c} + y_3 + d_3 + \Delta f_3) - \dot{g}_{2d} \end{aligned} \tag{49}$$

Thus

$$z_3 \dot{z}_3 = z_3 \left(\frac{\partial g_2}{\partial x_1} (f_1 + g_1 + d_1 + \Delta f_1) + \frac{\partial g_2}{\partial x_2} (f_2 + g_2 + \Delta f_2) - \dot{g}_{2d} \right) + \frac{\partial g_2}{\partial x_3} (f_3 + z_4 + g_{3c} + y_3 + d_3 + \Delta f_3) \tag{50}$$

RBFNN is introduced to approximate the nonlinearity Δf_3 in Equation (18). Ideally $\Delta f_3 = W_3^T \Phi_3(x_1, x_2, x_3) + \varepsilon_{\Delta_3}(x_1, x_2, x_3)$, and $\varepsilon_{\Delta_3}(x_1, x_2, x_3)$ is the RBFNN estimation error with an upper bound ε_{m_3} , then combining Lemmas 2, 3 and 5 yields

$$\begin{aligned} z_3 \Delta f_1 &= z_3 W_1^T \Phi_1(x_1) + z_3 \varepsilon_{\Delta_1}(x_1) \\ &\leq \|W_1^T\| \|z_3 \Phi_1(x_1)\| + \|z_3\| \varepsilon_{m_1} \leq \theta_1 z_3 \bar{\Phi}_{13} + \frac{1}{2} z_3^2 + \frac{1}{2} \varepsilon_{m_1}^2 \\ \bar{\Phi}_{13} &= \left(\frac{z_3 \Phi_1^T(x_1) \Phi_1(x_1)}{\sqrt{z_3^2 \Phi_1^T(x_1) \Phi_1(x_1) + \varepsilon_{13}^2}} + \varepsilon_{13} \right) \\ z_3 \Delta f_3 &= z_3 W_3^T \Phi_3(x_1, x_2, x_3) + z_3 \varepsilon_{\Delta_1}(x_1, x_2, x_3) \\ &\leq \|W_3^T\| \|z_3 \Phi_3(x_1, x_2, x_3)\| + \|z_3\| \varepsilon_{m_3} \leq \theta_3 z_3 \bar{\Phi}_{33} + \frac{1}{2} z_3^2 + \frac{1}{2} \varepsilon_{m_3}^2 \\ \bar{\Phi}_{33} &= \left(\frac{z_3 \Phi_3^T(x_1, x_2, x_3) \Phi_3(x_1, x_2, x_3)}{\sqrt{z_3^2 \Phi_3^T(x_1, x_2, x_3) \Phi_3(x_1, x_2, x_3) + \varepsilon_{33}^2}} + \varepsilon_{33} \right) \end{aligned} \tag{51}$$

where $\varepsilon_{13} > 0, \varepsilon_{33} > 0$ are parameters to be designed. Design the following control signals

$$g_{3c} = \frac{1}{\frac{\partial g_2}{\partial x_3}} \begin{pmatrix} -k_3 z_3 - \frac{\partial g_2}{\partial x_1} \left(f_1 + g_1 + \hat{D}_1 \tanh\left(\frac{z_1}{\varepsilon_{D_1}}\right) + \hat{\theta}_1 \bar{\Phi}_{13} \right) \\ -\frac{\partial g_2}{\partial x_2} \left(f_2 + g_2 + \hat{\Theta}_a^T \Psi_a(Z_a) \right) - \frac{y_2}{\tau_2} \\ -\frac{\partial g_2}{\partial x_3} \left(f_3 + \hat{\theta}_3 \bar{\Phi}_{33} + \hat{D}_3 \tanh\left(\frac{\partial g_2}{\partial x_3} \cdot \frac{z_3}{\varepsilon_{D_3}}\right) \right) \end{pmatrix} \tag{52}$$

where $k_3 > 0$ is a parameter to be designed.

Combining Equations (50)–(52), it can be known that

$$\begin{aligned} z_3 \dot{z}_3 &\leq -k_3 z_3^2 + \frac{\partial g_2}{\partial x_3} z_3 (z_4 + y_3) + \frac{\partial g_2}{\partial x_1} z_3 \left(d_1 - \hat{D}_1 \tanh\left(\frac{z_1}{\varepsilon_{D_1}}\right) \right) \\ &\quad - \frac{\partial g_2}{\partial x_1} z_3 \hat{\theta}_1 \bar{\Phi}_{13} - \frac{\partial g_2}{\partial x_2} z_3 \hat{\Theta}_a^T \Psi_a(Z_a) + \frac{\partial g_2}{\partial x_2} z_3 \varepsilon_a(Z_a) - \frac{\partial g_2}{\partial x_3} z_3 \hat{\theta}_3 \bar{\Phi}_{33} \\ &\quad + \frac{\partial g_2}{\partial x_3} z_3 \left(d_3 - \hat{D}_3 \tanh\left(\frac{\partial g_2}{\partial x_3} \cdot \frac{z_3}{\varepsilon_{D_3}}\right) \right) + z_3^2 + \frac{1}{2} \varepsilon_{m_1}^2 + \frac{1}{2} \varepsilon_{m_3}^2 \end{aligned} \tag{53}$$

Define the adaptive update law of \hat{D}_1 as

$$\dot{\hat{D}}_3 = \eta_{D_3} \frac{\partial g_2}{\partial x_3} z_3 \tanh\left(\frac{\partial g_2}{\partial x_3} \cdot \frac{z_3}{\varepsilon_{D_3}}\right) - \eta_{D_3} \sigma_{D_3} \hat{D}_3 \tag{54}$$

where $\eta_{D_3}, \sigma_{D_3} > 0$ are parameters to be designed.

3.1.4 Step 4

In view of eqnarray Equations (18), (21) and the forth formula of Equation (19), we have

$$\begin{aligned} \dot{z}_4 &= \dot{g}_3 - \dot{g}_{3d} \\ &= \frac{\partial g_3}{\partial x_1} \dot{x}_1 + \frac{\partial g_3}{\partial x_2} \dot{x}_2 + \frac{\partial g_3}{\partial x_3} \dot{x}_3 + \frac{\partial g_3}{\partial u} \dot{u} - \dot{g}_{3d} \\ &= \frac{\partial g_3}{\partial x_1} (f_1 + g_1 + d_1 + \Delta f_1) + \frac{\partial g_3}{\partial x_2} (f_2 + g_2 + \Delta f_2) \\ &\quad + \frac{\partial g_3}{\partial x_3} (f_3 + g_3 + d_3 + \Delta f_3) + \frac{\partial g_3}{\partial u} u_f - \dot{g}_{3d} \end{aligned} \tag{55}$$

Thus

$$z_4 \dot{z}_4 = z_4 \left[\frac{\partial g_3}{\partial x_1} (f_1 + g_1 + d_1 + \Delta f_1) + \frac{\partial g_3}{\partial x_2} (f_2 + g_2 + \Delta f_2) + \frac{\partial g_3}{\partial x_3} (f_3 + g_3 + d_3 + \Delta f_3) + \frac{\partial g_3}{\partial u} u_f - \dot{g}_{3d} \right] \tag{56}$$

With the aid of Lemmas 2, 3 and 5, it is obvious that

$$\begin{aligned} z_4 \Delta f_1 &= z_4 W_1^T \Phi_1(x_1) + z_4 \varepsilon_{\Delta_1}(x_1) \\ &\leq \|W_1^T\| \|z_4 \Phi_1(x_1)\| + \|z_4\| \varepsilon_{m1} \leq \theta_1 z_4 \bar{\Phi}_{14} + \frac{1}{2} z_4^2 + \frac{1}{2} \varepsilon_{m1}^2 \\ \bar{\Phi}_{14} &= \left(\frac{z_4 \Phi_1^T(x_1) \Phi_1(x_1)}{\sqrt{z_4^2 \Phi_1^T(x_1) \Phi_1(x_1) + \varepsilon_{14}^2}} + \varepsilon_{14} \right) \\ z_4 \Delta f_3 &= z_4^T \Phi_3(x_1, x_2, x_3) + z_4 \varepsilon_{\Delta_3}(x_1, x_2, x_3) \\ &\leq \|W_3^T\| \|z_4 \Phi_3(x_1, x_2, x_3)\| + \|z_4\| \varepsilon_{m3} \leq \theta_3 z_4 \bar{\Phi}_{34} + \frac{1}{2} z_4^2 + \frac{1}{2} \varepsilon_{m3}^2 \\ \bar{\Phi}_{34} &= \left(\frac{z_4 \Phi_3^T(x_1, x_2, x_3) \Phi_3(x_1, x_2, x_3)}{\sqrt{z_4^2 \Phi_3^T(x_1, x_2, x_3) \Phi_3(x_1, x_2, x_3) + \varepsilon_{34}^2}} + \varepsilon_{34} \right) \end{aligned} \tag{57}$$

where $\varepsilon_{14} > 0, \varepsilon_{34} > 0$ are parameters to be designed. Select the final actual control law u_f as

$$u_f = \frac{1}{\frac{\partial g_3}{\partial u}} \left(-\frac{\partial g_3}{\partial x_1} \left(f_1 + g_1 + \hat{D}_1 \tanh\left(\frac{z_1}{\varepsilon_{D_1}}\right) + \hat{\theta}_1 \bar{\Phi}_{14} \right) - \frac{\partial g_3}{\partial x_2} \left(f_2 + g_2 + \hat{\Theta}_a^T \Psi_a(Z_a) \right) \right. \\ \left. - \frac{\partial g_3}{\partial x_3} \left(f_3 + g_3 + \hat{D}_3 \tanh\left(\frac{\partial g_2}{\partial x_3} \cdot \frac{z_3}{\varepsilon_{D_3}}\right) + \hat{\theta}_3 \bar{\Phi}_{34} \right) - k_4 z_4 - \frac{v_3}{\tau_3} \right) \tag{58}$$

where $k_4 > 0$ is a positive parameter to be designed.

In view of Equations (56)–(58), it can be known that

$$\begin{aligned} z_4 \dot{z}_4 &\leq -k_4 z_4^2 + z_4^2 - \frac{\partial g_3}{\partial x_1} z_4 \tilde{\theta}_1 \bar{\Phi}_{14} - \frac{\partial g_3}{\partial x_2} z_4 \tilde{\Theta}_a^T \Psi_a(Z_a) \\ &\quad + \frac{\partial g_3}{\partial x_2} z_4 \varepsilon_a(Z_a) - \frac{\partial g_3}{\partial x_3} z_4 \tilde{\theta}_3 \bar{\Phi}_{34} + \frac{1}{2} \varepsilon_{m1}^2 + \frac{1}{2} \varepsilon_{m3}^2 \\ &\quad + \frac{\partial g_3}{\partial x_1} z_4 \left(d_1 - \hat{D}_1 \tanh\left(\frac{z_1}{\varepsilon_{D_1}}\right) \right) + \frac{\partial g_3}{\partial x_3} z_4 \left(d_3 - \hat{D}_3 \tanh\left(\frac{\partial g_2}{\partial x_3} \cdot \frac{z_3}{\varepsilon_{D_3}}\right) \right) \end{aligned} \tag{59}$$

Last but not least, we select the following adaptive update laws of $\hat{\theta}_1$ and $\hat{\theta}_3$

$$\begin{aligned} \dot{\hat{\theta}}_1 &= \eta_1 \left(z_1 \bar{\Phi}_{11} + \frac{\partial g_1}{\partial x_1} z_2 \bar{\Phi}_{12} + \frac{\partial g_2}{\partial x_1} z_3 \bar{\Phi}_{13} + \frac{\partial g_3}{\partial x_1} z_4 \bar{\Phi}_{14} \right) - \eta_1 \sigma_1 \hat{\theta}_1 \\ \dot{\hat{\theta}}_3 &= \eta_3 \left(\frac{\partial g_2}{\partial x_3} z_3 \bar{\Phi}_{33} + \frac{\partial g_3}{\partial x_3} z_4 \bar{\Phi}_{34} \right) - \eta_3 \sigma_3 \hat{\theta}_3 \end{aligned} \tag{60}$$

where $\eta_1, \eta_3 > 0$ are the gains of the adaptive update laws and $\sigma_1, \sigma_3 > 0$ are parameters to be designed.

3.2 Analysis of stability

Theorem 1. *Considering the NAIGC system (7) in the presence of actuator faults and unknown uncertainties, the controller (58), the parameter update laws (30), (54), the gradient descent update laws (36), (45) and the adaptive update law (60). Suppose that Assumptions 1, 2 are satisfied, and the error of the hyperbolic tangent function estimation disturbance is bounded. Then the following conclusions hold*

- The output guidance strategy of the system eventually converges to near zero, i.e., precision guided interception can be achieved.
- The boundedness of all signals can be guaranteed and the tracking error converges to zero.

We construct the Lyapunov function

$$V = \sum_{i=1}^4 \frac{1}{2} z_i^2 + \sum_{i=1}^3 \frac{1}{2} y_i^2 + \sum_{i=1,3} \frac{1}{2\eta_i} \tilde{\theta}_i^2 + \sum_{i=1,3} \frac{1}{2\eta_{D_i}} \tilde{D}_i^2 + \frac{1}{2} \tilde{\Theta}_a^T \eta_a^{-1} \tilde{\Theta}_a + \frac{1}{2} \tilde{\Theta}_J^T \eta_J^{-1} \tilde{\Theta}_J \tag{61}$$

Combining Equations (22), (29), (53), (59) we can take the derivative of $V(t)$ as

$$\begin{aligned} \dot{V} &= z_1 \dot{z}_1 + z_2 \dot{z}_2 + z_3 \dot{z}_3 + z_4 \dot{z}_4 + y_1 \dot{y}_1 + y_2 \dot{y}_2 + y_3 \dot{y}_3 + \frac{1}{2} \dot{z}_1^2 + \frac{1}{2} \dot{z}_2^2 + \dot{z}_3^2 + \dot{z}_4^2 \\ &+ \frac{1}{\eta_{D_1}} \tilde{D}_1 \dot{\tilde{D}}_1 + \frac{1}{\eta_{D_3}} \tilde{D}_3 \dot{\tilde{D}}_3 + \frac{1}{\eta_1} \tilde{\theta}_1 \dot{\tilde{\theta}}_1 + \frac{1}{\eta_3} \tilde{\theta}_3 \dot{\tilde{\theta}}_3 + \tilde{\Theta}_a^T \eta_a^{-1} \dot{\tilde{\Theta}}_a + \tilde{\Theta}_J^T \eta_J^{-1} \dot{\tilde{\Theta}}_J \\ &\leq -k_1 z_1^2 - k_2 z_2^2 - k_3 z_3^2 - k_4 z_4^2 - \left(\frac{\partial g_1}{\partial x_2} z_2 + \frac{\partial g_2}{\partial x_2} z_3 + \frac{\partial g_3}{\partial x_2} z_4 \right) \left(\tilde{\Theta}_a^T \Psi_a(Z_a) - \varepsilon_a \right) \\ &+ z_1 \left(d_1 - \hat{D}_1 \tanh \left(\frac{z_1}{\varepsilon_{D_1}} \right) \right) + \left(\frac{\partial g_1}{\partial x_1} z_2 + \frac{\partial g_2}{\partial x_1} z_3 + \frac{\partial g_3}{\partial x_1} z_4 \right) \left(d_1 - \hat{D}_1 \tanh \left(\frac{z_1}{\varepsilon_{D_1}} \right) \right) \\ &+ \frac{\partial g_2}{\partial x_3} z_3 \left(d_3 - \hat{D}_3 \tanh \left(\frac{\partial g_2}{\partial x_3} \cdot \frac{z_3}{\varepsilon_{D_3}} \right) \right) + \frac{\partial g_3}{\partial x_3} z_4 \left(d_3 - \hat{D}_3 \tanh \left(\frac{\partial g_2}{\partial x_3} \cdot \frac{z_3}{\varepsilon_{D_3}} \right) \right) \\ &- \left(z_1 \bar{\Phi}_{11} + \frac{\partial g_1}{\partial x_1} z_2 \bar{\Phi}_{12} + \frac{\partial g_2}{\partial x_1} z_3 \bar{\Phi}_{13} + \frac{\partial g_3}{\partial x_1} z_4 \bar{\Phi}_{14} \right) \tilde{\theta}_1 - \left(\frac{\partial g_2}{\partial x_3} z_3 \bar{\Phi}_{33} + \frac{\partial g_3}{\partial x_3} z_4 \bar{\Phi}_{34} \right) \tilde{\theta}_3 \\ &+ z_1 (z_2 + y_1) + \frac{\partial g_1}{\partial x_2} z_2 (z_3 + y_2) + \frac{\partial g_2}{\partial x_3} z_3 (z_4 + y_3) + \tilde{\Theta}_a^T \eta_a^{-1} \dot{\tilde{\Theta}}_a + \tilde{\Theta}_J^T \eta_J^{-1} \dot{\tilde{\Theta}}_J + 2\varepsilon_{m1}^2 + \varepsilon_{m3}^2 \\ &- \frac{y_1^2}{\tau_1} - \dot{g}_{1c} y_1 - \frac{y_2^2}{\tau_2} - \dot{g}_{2c} y_2 - \frac{y_3^2}{\tau_3} - \dot{g}_{3c} y_3 + \frac{1}{\eta_{D_1}} \tilde{D}_1 \dot{\tilde{D}}_1 + \frac{1}{\eta_{D_3}} \tilde{D}_3 \dot{\tilde{D}}_3 + \frac{1}{\eta_1} \tilde{\theta}_1 \dot{\tilde{\theta}}_1 + \frac{1}{\eta_3} \tilde{\theta}_3 \dot{\tilde{\theta}}_3 \end{aligned} \tag{62}$$

According to Lemma 1, we can obtain that

$$\begin{aligned} z_1 d_1 \leq |z_1 d_1| &\leq D_1 \left(z_1 \tanh \left(\frac{z_1}{\varepsilon_{D_1}} \right) + \kappa \varepsilon_{D_1} \right) \frac{\partial g_2}{\partial x_3} z_3 \left(d_3 - \hat{D}_3 \tanh \left(\frac{\partial g_2}{\partial x_3} \cdot \frac{z_3}{\varepsilon_{D_3}} \right) \right) \\ &\leq -\tilde{D}_3 \frac{\partial g_2}{\partial x_3} z_3 \tanh \left(\frac{\partial g_2}{\partial x_3} \cdot \frac{z_3}{\varepsilon_{D_3}} \right) + D_3 \kappa \varepsilon_{D_3} \end{aligned} \tag{63}$$

Consequently, the sixth and eighth items of Equation (62) satisfy the following inequality

$$z_1 \left(d_1 - \hat{D}_1 \tanh \left(\frac{z_1}{\varepsilon_{D_1}} \right) \right) \leq -\tilde{D}_1 z_1 \tanh \left(\frac{z_1}{\varepsilon_{D_1}} \right) + D_1 \varepsilon_{D_1}$$

$$\frac{\partial g_2}{\partial x_3} z_3 \left(d_3 - \hat{D}_3 \tanh \left(\frac{\partial g_2}{\partial x_3} \cdot \frac{z_3}{\varepsilon_{D_3}} \right) \right) \leq -\tilde{D}_3 \frac{\partial g_2}{\partial x_3} z_3 \tanh \left(\frac{\partial g_2}{\partial x_3} \cdot \frac{z_3}{\varepsilon_{D_3}} \right) + D_3 \kappa \varepsilon_{D_3} \tag{64}$$

Combining Assumption 1 and Equations (24), (48), the seventh and ninth items of Equation (62) satisfy

$$\left(\frac{\partial g_1}{\partial x_1} z_2 + \frac{\partial g_2}{\partial x_1} z_3 + \frac{\partial g_3}{\partial x_1} z_4 \right) \left(d_1 - \hat{D}_1 \tanh \left(\frac{z_1}{\varepsilon_{D_1}} \right) \right) \leq \frac{1}{2} \bar{g}^2 z_2^2 + \frac{1}{2} \bar{g}^2 z_3^2 + \frac{1}{2} \bar{g}^2 z_4^2 + \frac{3}{2} \bar{\varepsilon}_{D_1}^2$$

$$\frac{\partial g_3}{\partial x_3} z_4 \left(d_3 - \hat{D}_3 \tanh \left(\frac{\partial g_2}{\partial x_3} \cdot \frac{z_3}{\varepsilon_{D_3}} \right) \right) \leq \frac{1}{2} \bar{g}^2 z_4^2 + \frac{1}{2} \bar{\varepsilon}_{D_3}^2 \tag{65}$$

With Equations (64), (65) and the update laws (30), (43), (36), (54), Equation (62) can be rewritten as

$$\begin{aligned} \dot{V} \leq & -k_1 z_1^2 - k_2 z_2^2 - k_3 z_3^2 - k_4 z_4^2 - \sigma_a \tilde{\Theta}_a^T \hat{\Theta}_a - \sigma_J \tilde{\Theta}_J^T \hat{\Theta}_J + \frac{1}{2} z_1^2 + \frac{1}{2} z_2^2 + z_3^2 + z_4^2 \\ & - \sigma_{D_1} \tilde{D}_1 \hat{D}_1 + D_1 \kappa \varepsilon_{D_1} - \sigma_{D_3} \tilde{D}_3 \hat{D}_3 + D_3 \kappa \varepsilon_{D_3} + \frac{1}{2} \bar{g}^2 z_2^2 + \frac{1}{2} \bar{g}^2 z_3^2 + \frac{1}{2} \bar{g}^2 z_4^2 + \frac{1}{2} \bar{g}^2 z_4^2 \\ & - \sigma_1 \tilde{\theta}_1 \hat{\theta}_1 - \sigma_3 \tilde{\theta}_3 \hat{\theta}_3 + z_1 (z_2 + y_1) + \frac{\partial g_1}{\partial x_2} z_2 (z_3 + y_2) + \frac{\partial g_2}{\partial x_3} z_3 (z_4 + y_3) \\ & - \frac{y_1^2}{\tau_1} - \dot{g}_{1c} y_1 - \frac{y_2^2}{\tau_2} - \dot{g}_{2c} y_2 - \frac{y_3^2}{\tau_3} - \dot{g}_{3c} y_3 + 2\varepsilon_{m1}^2 + \varepsilon_{m3}^2 + \frac{3}{2} \bar{\varepsilon}_{D_1}^2 + \frac{1}{2} \bar{\varepsilon}_{D_3}^2 \\ & - \left(\frac{\partial g_1}{\partial x_2} z_2 + \frac{\partial g_2}{\partial x_2} z_3 + \frac{\partial g_3}{\partial x_2} z_4 \right) \tilde{\Theta}_a^T \Psi_a (Z_a) + \left(\frac{\partial g_1}{\partial x_2} z_2 + \frac{\partial g_2}{\partial x_2} z_3 + \frac{\partial g_3}{\partial x_2} z_4 \right) \varepsilon_a \\ & - \frac{\partial g_1}{\partial x_2} \left(\frac{\partial g_1}{\partial x_2} \hat{\Theta}_a^T \Psi_a (Z_a) + \hat{J} \right) \tilde{\Theta}_a^T \Psi_a (Z_a) - \varepsilon_{critic} \tilde{\Theta}_J^T \dot{\Psi}_J (Z_c) \end{aligned} \tag{66}$$

In view of inequality $2ab \leq a^2 + b^2$ and Assumption 1 we have

$$z_1 (z_2 + y_1) + \frac{\partial g_1}{\partial x_2} z_2 (z_3 + y_2) + \frac{\partial g_2}{\partial x_3} z_3 (z_4 + y_3)$$

$$\leq z_1^2 + \left(\frac{1}{2} + \bar{g}^2 \right) z_2^2 + \left(\frac{1}{2} + \bar{g}^2 \right) z_3^2 + \frac{1}{2} z_4^2 + \frac{1}{2} y_1^2 + \frac{1}{2} y_2^2 + \frac{1}{2} y_3^2 \tag{67}$$

According to Lemma 3, we can get that

$$-\dot{g}_{1c} y_1 \leq \frac{y_1^2}{2\tau_1} + \frac{\tau_1 |\dot{g}_{1c}|^2}{2}$$

$$-\dot{g}_{2c} y_2 \leq \frac{y_2^2}{2\tau_2} + \frac{\tau_2 |\dot{g}_{2c}|^2}{2} \tag{68}$$

$$-\dot{g}_{3c} y_3 \leq \frac{y_3^2}{2\tau_3} + \frac{\tau_3 |\dot{g}_{3c}|^2}{2}$$

Substituting Equations (67), (68) into Equation (66) yields that

$$\begin{aligned}
 \dot{V} \leq & -\left(k_1 - \frac{3}{2}\right) z_1^2 - \left(k_2 - 1 - \frac{3}{2}\bar{g}^2\right) z_2^2 - \left(k_3 - \frac{3}{2} - \frac{3}{2}\bar{g}^2\right) z_3^2 - \left(k_4 - \frac{3}{2} - \bar{g}^2\right) z_4^2 \\
 & - \sum_{i=1}^3 \left(\frac{1}{2\tau_i} - \frac{1}{2}\right) y_i^2 - \frac{\partial g_1}{\partial x_2} \left(\frac{\partial g_1}{\partial z_2} \hat{\Theta}_a^T \Psi_a(Z_a) + \hat{J}\right) \tilde{\Theta}_a^T \Psi_a(Z_a) - \varepsilon_{critic} \tilde{\Theta}_J^T \dot{\Psi}_J(Z_c) \\
 & - \left(\frac{\partial g_1}{\partial x_2} z_2 + \frac{\partial g_2}{\partial x_2} z_3 + \frac{\partial g_3}{\partial x_2} z_4\right) \tilde{\Theta}_a^T \Psi_a(Z_a) + \left(\frac{\partial g_1}{\partial x_2} z_2 + \frac{\partial g_2}{\partial x_2} z_3 + \frac{\partial g_3}{\partial x_2} z_4\right) \varepsilon_a \\
 & - \sigma_a \tilde{\Theta}_a^T \hat{\Theta}_a - \sigma_J \tilde{\Theta}_J^T \hat{\Theta}_J - \sigma_{D_1} \tilde{D}_1 \hat{D}_1 - \sigma_{D_3} \tilde{D}_3 \hat{D}_3 - \sigma_1 \tilde{\theta}_1 \hat{\theta}_1 - \sigma_3 \tilde{\theta}_3 \hat{\theta}_3 \\
 & + D_1 \kappa \varepsilon_{D_1} + D_3 \kappa \varepsilon_{D_3} + \frac{3}{2} \bar{\varepsilon}_{D_1}^2 + \frac{1}{2} \bar{\varepsilon}_{D_3}^2 + \sum_{i=1}^3 \frac{\tau_i}{2} |\dot{g}_{ic}|^2 + 2\varepsilon_{m1}^2 + \varepsilon_{m3}^2
 \end{aligned} \tag{69}$$

Based on Assumption 2, we can know that $\|\Psi_a\| \leq \psi_a, \|\Psi_J\| \leq \psi_J$. The sixth term of Equation (69) can be calculated that

$$\begin{aligned}
 & - \frac{\partial g_1}{\partial x_2} \left(\frac{\partial g_1}{\partial x_2} \hat{\Theta}_a^T \Psi_a(Z_a) + \hat{J}\right) \tilde{\Theta}_a^T \Psi_a(Z_a) \\
 = & - \left(\frac{\partial g_1}{\partial x_2}\right)^2 \tilde{\Theta}_a^T \Psi_a(Z_a) \hat{\Theta}_a^T \Psi_a(Z_a) - \frac{\partial g_1}{\partial x_2} \tilde{\Theta}_a^T \Psi_a(Z_a) \hat{\Theta}_J^T \Psi_J(Z_c) \\
 = & - \left(\frac{\partial g_1}{\partial x_2}\right)^2 \tilde{\Theta}_a^T \Psi_a(Z_a) \Theta_a^T \Psi_a(Z_a) - \left(\frac{\partial g_1}{\partial x_2}\right)^2 \tilde{\Theta}_a^T \Psi_a(Z_a) \tilde{\Theta}_a^T \Psi_a(Z_a) \\
 & - \frac{\partial g_1}{\partial x_2} \tilde{\Theta}_a^T \Psi_a(Z_a) \Theta_J^T \Psi_J(Z_c) - \frac{\partial g_1}{\partial x_2} \tilde{\Theta}_a^T \Psi_a(Z_a) \tilde{\Theta}_J^T \Psi_J(Z_c) \\
 \leq & \frac{1}{2} \bar{g}^2 \left(\tilde{\Theta}_a^T \Psi_a(Z_a)\right)^2 + \frac{1}{2} \bar{g}^2 \left(\Theta_a^T \Psi_a(Z_a)\right)^2 + \bar{g} \left(\tilde{\Theta}_a^T \Psi_a(Z_a)\right)^2 \\
 & + \frac{1}{2} \bar{g} \left(\Theta_J^T \Psi_J(Z_c)\right)^2 + \frac{1}{2} \bar{g} \left(\tilde{\Theta}_J^T \Psi_J(Z_c)\right)^2 \\
 \leq & \frac{1}{2} \bar{g}^2 \psi_a^2 \left\|\tilde{\Theta}_a\right\|^2 + \frac{1}{2} \bar{g}^2 \psi_a^2 \left\|\Theta_a\right\|^2 + \bar{g} \psi_a^2 \left\|\tilde{\Theta}_a\right\|^2 + \frac{1}{2} \bar{g} \psi_J^2 \left\|\Theta_J\right\|^2 + \frac{1}{2} \bar{g} \psi_J^2 \left\|\tilde{\Theta}_J\right\|^2
 \end{aligned} \tag{70}$$

Based on Assumption 2, we can know that $\|\dot{\Psi}_J\| \leq \gamma_J, |\dot{\varepsilon}_J| \leq \xi_J$. The seventh term of Equation (69) holds

$$\begin{aligned}
 & - \varepsilon_{critic} \tilde{\Theta}_J^T \dot{\Psi}_J(Z_c) = - \left(\Theta_J^T \dot{\Psi}_J(Z_c) + \dot{\varepsilon}_J + \hat{\Theta}_J^T \dot{\Psi}_J(Z_c)\right) \tilde{\Theta}_J^T \dot{\Psi}_J(Z_c) \\
 = & - \Theta_J^T \dot{\Psi}_J(Z_c) \tilde{\Theta}_J^T \dot{\Psi}_J(Z_c) - \dot{\varepsilon}_J \tilde{\Theta}_J^T \dot{\Psi}_J(Z_c) - \left(\Theta_J^T + \tilde{\Theta}_J^T\right) \dot{\Psi}_J(Z_c) \tilde{\Theta}_J^T \dot{\Psi}_J(Z_c) \\
 = & -2\Theta_J^T \dot{\Psi}_J(Z_c) \tilde{\Theta}_J^T \dot{\Psi}_J(Z_c) - \dot{\varepsilon}_J \tilde{\Theta}_J^T \dot{\Psi}_J(Z_c) - \tilde{\Theta}_J^T \dot{\Psi}_J(Z_c) \tilde{\Theta}_J^T \dot{\Psi}_J(Z_c) \\
 \leq & \left\|-\Theta_J^T \dot{\Psi}_J(Z_c)\right\|^2 + \left\|\tilde{\Theta}_J^T \dot{\Psi}_J(Z_c)\right\|^2 - \left\|\tilde{\Theta}_J^T \dot{\Psi}_J(Z_c)\right\|^2 + \frac{1}{2} \left\|\tilde{\Theta}_J^T \dot{\Psi}_J(Z_c)\right\|^2 + \frac{1}{2} (-\dot{\varepsilon}_J)^2 \\
 \leq & \frac{1}{2} \gamma_J^2 \left\|\tilde{\Theta}_J\right\|^2 + \gamma_J^2 \left\|\Theta_J\right\|^2 + \frac{1}{2} \xi_J^2
 \end{aligned} \tag{71}$$

Based on Assumption 2, we can know that $|\varepsilon_a| \leq \varsigma_a$. The eighth and ninth items of Equation (69) can be formulated that

$$\begin{aligned} & - \left(\frac{\partial g_1}{\partial x_2} z_2 + \frac{\partial g_2}{\partial x_2} z_3 + \frac{\partial g_3}{\partial x_2} z_4 \right) \tilde{\Theta}_a^T \Psi_a(Z_a) + \left(\frac{\partial g_1}{\partial x_2} z_2 + \frac{\partial g_2}{\partial x_2} z_3 + \frac{\partial g_3}{\partial x_2} z_4 \right) \varepsilon_a \\ & \leq \bar{g} \left(|z_2 \tilde{\Theta}_a^T \Psi_a(Z_a)| + |z_3 \tilde{\Theta}_a^T \Psi_a(Z_a)| + |z_4 \tilde{\Theta}_a^T \Psi_a(Z_a)| + (|z_2| + |z_3| + |z_4|) \cdot |\varepsilon_a| \right) \\ & \leq \bar{g} \left(z_2^2 + z_3^2 + z_4^2 + \frac{3}{2} \psi_a^2 \|\tilde{\Theta}_a\|^2 + \frac{3}{2} \varsigma_a^2 \right) \end{aligned} \tag{72}$$

Considering the following inequality

$$\begin{aligned} -\sigma_a \tilde{\Theta}_a^T \hat{\Theta}_a & \leq -\frac{\sigma_a}{2} \|\tilde{\Theta}_a\|^2 + \frac{\sigma_a}{2} \|\Theta_a\|^2 \\ -\sigma_J \tilde{\Theta}_J^T \hat{\Theta}_J & \leq -\frac{\sigma_J}{2} \|\tilde{\Theta}_J\|^2 + \frac{\sigma_J}{2} \|\Theta_J\|^2 \\ -\sigma_{D_1} \tilde{D}_1 \hat{D}_1 & \leq -\frac{1}{2} \sigma_{D_1} \tilde{D}_1^2 + \frac{1}{2} \sigma_{D_1} D_1^2 \\ -\sigma_{D_3} \tilde{D}_3 \hat{D}_3 & \leq -\frac{1}{2} \sigma_{D_3} \tilde{D}_3^2 + \frac{1}{2} \sigma_{D_3} D_3^2 \\ -\sigma_1 \tilde{\theta}_1 \hat{\theta}_1 & \leq -\frac{1}{2} \sigma_1 \tilde{\theta}_1^2 + \frac{1}{2} \sigma_1 \theta_1^2 \\ -\sigma_3 \tilde{\theta}_3 \hat{\theta}_3 & \leq -\frac{1}{2} \sigma_3 \tilde{\theta}_3^2 + \frac{1}{2} \sigma_3 \theta_3^2 \end{aligned} \tag{73}$$

Combining Equations (70)–(73), we can finally draw the following conclusion

$$\begin{aligned} \dot{V} & \leq - \left(k_1 - \frac{3}{2} \right) z_1^2 - \left(k_2 - 1 - \bar{g} - \frac{3}{2} \bar{g}^2 \right) z_2^2 - \left(k_3 - \frac{3}{2} - \bar{g} - \frac{3}{2} \bar{g}^2 \right) z_3^2 - \left(k_4 - \frac{3}{2} - \bar{g} - \bar{g}^2 \right) z_4^2 \\ & - \sum_{i=1}^3 \left(\frac{1}{2\tau_i} - \frac{1}{2} \right) y_i^2 - \frac{1}{2} (\sigma_a - 5\bar{g}\psi_a^2 - \bar{g}^2\psi_a^2) \|\tilde{\Theta}_a\|^2 - \frac{1}{2} (\sigma_J - \gamma_J^2 - \bar{g}\psi_J^2) \|\tilde{\Theta}\|^2 \\ & - \sum_{i=1,3} \frac{1}{2} \sigma_{D_i} \tilde{D}_i^2 - \sum_{i=1}^3 \frac{1}{2} \sigma_i \tilde{W}_i^T \tilde{W}_i \\ & \leq -C_V V + E_V \end{aligned} \tag{74}$$

where

$$\begin{aligned} C_V & = \min \left\{ 2 \left(k_1 - \frac{3}{2} \right), 2 \left(k_2 - 1 - \bar{g} - \frac{3}{2} \bar{g}^2 \right), 2 \left(k_3 - \frac{3}{2} - \bar{g} - \frac{3}{2} \bar{g}^2 \right), 2 \left(k_4 - \frac{3}{2} - \bar{g} - \bar{g}^2 \right), \right. \\ & \left. \left(\frac{1}{\tau_1} - 1 \right), \left(\frac{1}{\tau_2} - 1 \right), \left(\frac{1}{\tau_3} - 1 \right), \eta_a (\sigma_a - 5\bar{g}\psi_a^2 - \bar{g}^2\psi_a^2), \eta_J (\sigma_J - \gamma_J^2 - \bar{g}\psi_J^2), \right. \\ & \left. \eta_{D_1} \sigma_{D_1}, \eta_{D_3} \sigma_{D_3}, \eta_1 \sigma_1, \eta_3 \sigma_3 \right\} \\ E_V & = D_1 \kappa \varepsilon_{D_1} + D_3 \kappa \varepsilon_{D_3} + \frac{3}{2} \bar{\varepsilon}_{D_1}^2 + \frac{1}{2} \bar{\varepsilon}_{D_3}^2 + \sum_{i=1,3} \frac{1}{2} \sigma_{D_i} D_i^2 \\ & + \left(\frac{\sigma_a}{2} + \frac{1}{2} \bar{g}^2 \psi_a^2 \right) \|\Theta_a\|^2 + \frac{3}{2} \bar{g} \varsigma_a^2 + \left(\frac{\sigma_J}{2} + \frac{1}{2} \bar{g} \psi_J^2 + \gamma_J^2 \right) \|\Theta_J\|^2 + \frac{1}{2} \xi_J^2 \\ & + \sum_{i=1}^3 \frac{\tau_i}{2} |\dot{g}_{ic}|^2 + \sum_{i=1,3} \frac{1}{2} \sigma_i \theta_i^2 + 2\varepsilon_{m1}^2 + \varepsilon_{m3}^2 \end{aligned} \tag{75}$$

Table 1. Target location in different situations

	Target location	The range along theline of sight (LOS)	Line-of-sight angle
Case 1	$x_T = 6,000, y_T = 7,000$	$r(0) = 9,219.54m$	$\lambda = 0.86rad$
Case 2	$x_T = 7,000, y_T = 8,000$	$r(0) = 10,630.14m$	$\lambda = 0.85rad$
Case 3	$x_T = 8,000, y_T = 9,000$	$r(0) = 12,041.59m$	$\lambda = 0.84rad$

Table 2. The actuator failures in different situations

	λ_δ	d_δ
Case 1	$\lambda_\delta = 1$	$d_\delta = 0.01$
Case 2	$\lambda_\delta = 0.95 + 0.01\cos(6.28*t)$	$d_\delta = 0.01\sin(3.14*t)$
Case 3	$t > 2, \lambda_\delta = 0.5 + 0.01\cos(3.14*t)$ $t > 4, \lambda_\delta = 0.4 + 0.02\sin(6.28*t)$	$t > 2, d_\delta = 0.02\sin(6.28*t)$ $t > 4, d_\delta = 0.01\cos(3.14*t)$

Table 3. The target accelerations in different situations

	$A_{T\lambda}$	A_{Tr}
Case 1	$A_{T\lambda} = 10$	$A_{Tr} = 5$
Case 2	$A_{T\lambda} = 10 + 5\sin(6.28*t)$	$A_{Tr} = 15\sin(3.14*t)$
Case 3	$t > 2, A_{T\lambda} = 20 + 5\sin(6.28/0.22*t)$ $t > 4, A_{T\lambda} = 15 + 2\sin(1/0.22*t)$	$t > 2, A_{Tr} = 15\sin(62.8*t)$ $t > 4, A_{Tr} = 10\sin(10*t)$

According to Lemma 4, $V(t)$ is bounded. Hence, the parameters in $V(t)$ are bounded. Furthermore, the control signals are convergent and bounded so that we can draw the conclusion that the NAIGC system is stable. The proof is completed.

4.0 Simulation

In this paper, the validity and effectiveness of the proposed method are verified by numerical simulations. The effectiveness of the proposed method is verified by designing simulations considering the time-varying maneuver acceleration of the target and the time-varying actuator failure of the missile flight control. The robustness of the proposed method is also verified by comparing it with actor-critic without reinforcement learning.

The initial conditions of the missile kinematic eqnarrays and the initial velocity of the target are given in Ref. [10]. The aerodynamic and body parameters of the missile are given in Ref. [10] and the angle of the elevator is limited to $[-30^\circ, 30^\circ]$. The initial position of the missile is set as follows: $x(0) = 0m, y(0) = 0m$. The flight path angle of the target is initialised $\gamma_T(0) = 0$. The initial conditions for the actuator fault output are as follows: $\lambda_\delta(0) = 1, u(0) = 0, d_\delta(0) = 0$. The initial values for the adaptive parameters and neural network related parameters in the control step are as follows:

$$\hat{D}_1(0) = 10, \hat{D}_3(0) = 0, \hat{\theta}_1(0) = \hat{\theta}_2(0) = \hat{\theta}_3(0) = 0$$

$$\hat{\Theta}_a(0) = [0.2, 0.6, -0.3, 0.1, -0.5, 0.8, 0.15, -0.23, 0.35]$$

$$\hat{\Theta}_j(0) = [0.3, 0.1, -0.7, 0.5, -0.64, 0.28, 0.85, -0.23, 0.35, -0.11, -0.92]$$

Different initial positions of the targets under different conditions, different actuator failures, different time-varying target maneuver acceleration A_{Tr} and $A_{T\lambda}$. Specific parameters are shown in Tables 1, 2 and 3, respectively. The control gain is set to $k_1 = 5, k_2 = 20, k_3 = 40, k_4 = 150$; The parameters of the bounders of the tanh function are chosen as $\varepsilon_{D_1} = 500, \varepsilon_{D_3} = 100$; The parameters of the actor-critic network weight gradient descent update law are chosen as $\eta_a = 0.1, \sigma_a = 50, \eta_j = 0.1, \sigma_j = 50$. The

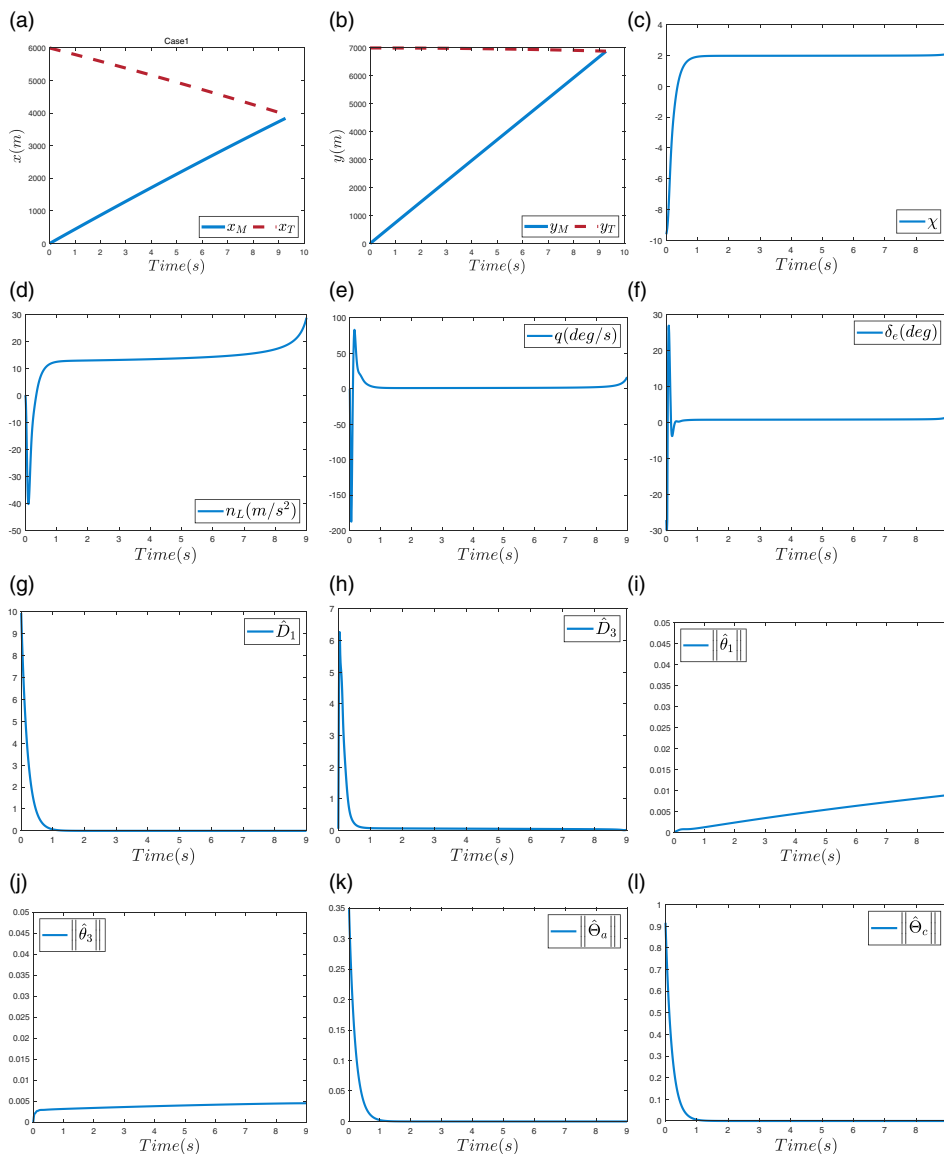


Figure 3. Simulation profiles for Case 1. (a) The x coordinates of missile and target. (b) The y coordinates of missile and target. (c) The guide variable χ . (d) The normal acceleration n_L of missile. (e) The pitch rate q of missile. (f) The actuator output δ_c . (g) The estimate of the upper bound of the interference norm D_1 . (h) The estimate of the upper bound of the interference norm D_3 . (i) The paradigm of the parameter θ_1 estimate. (j) The paradigm of the parameter θ_3 estimate. (k) The actor network weight norm. (l) The critic network weight norm.

parameters of the adaptive update law are chosen as $\eta_{D_1} = 0.01, \sigma_{D_1} = 20, \eta_{D_3} = 0.001, \sigma_{D_3} = 1e4, \eta_1 = 0.001, \sigma_1 = 50, \eta_3 = 5e - 7, \sigma_3 = 10$; The parameters of the filter are chosen as $\tau_1 = 0.2, \tau_2 = \tau_3 = 0.1$. The other parameters are $c_0 = 0.1, \epsilon_{11} = \epsilon_{12} = \epsilon_{13} = \epsilon_{33} = \epsilon_{14} = \epsilon_{34} = 1$.

The simulation results for Case 1, Case 2 and Case 3 are shown in Figs 3, 4 and 5, respectively. The horizontal coordinates of the missile and the target in the two-dimensional plane are shown in Figs 3(a), 4(a) and 5(a). The vertical coordinates of the missile and the target in the two-dimensional plane are shown in Figs 3(b), 4(b) and 5(b). Figures 3(c), 4(c) and 5(c) show the system output y (guide variable

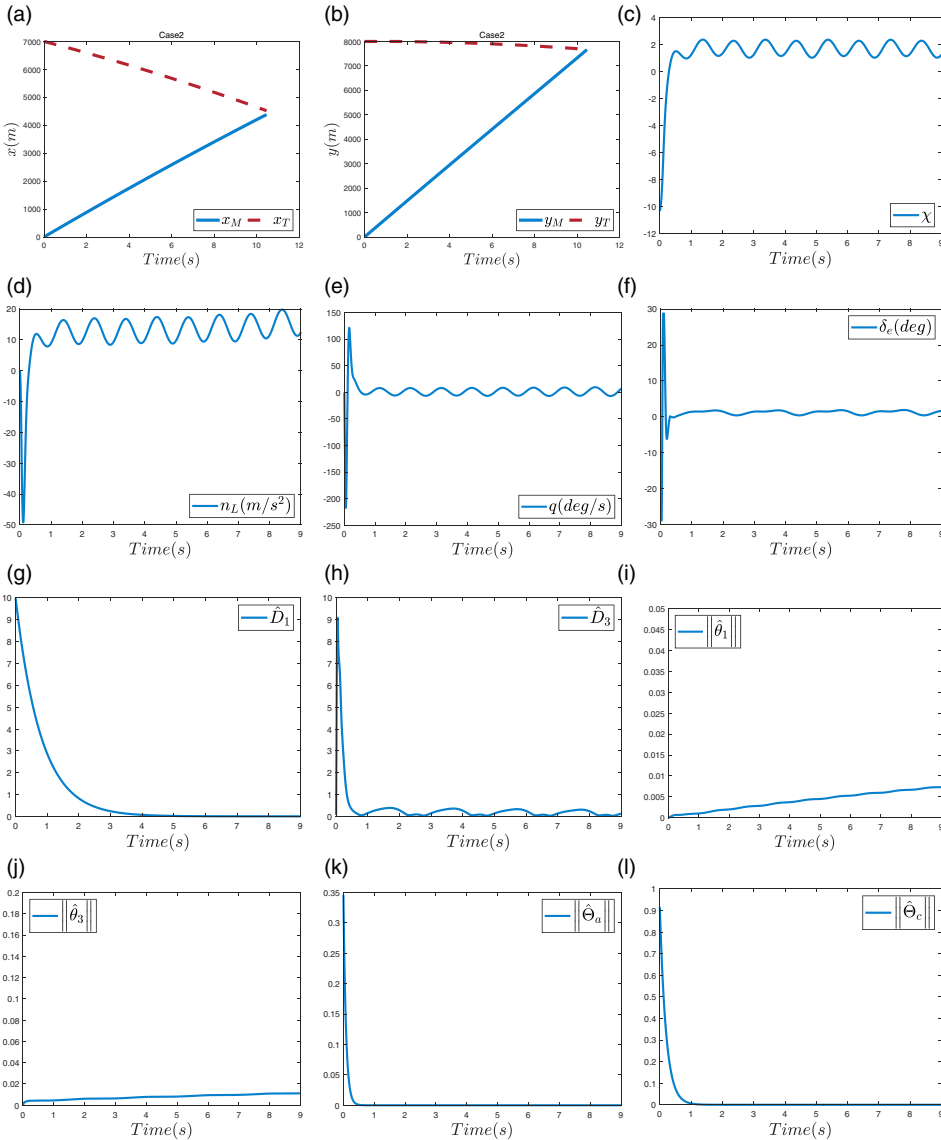


Figure 4. Simulation profiles for Case 2. (a) The x coordinates of missile and target. (b) The y coordinates of missile and target. (c) The guide variable χ . (d) The normal acceleration n_L of missile. (e) The pitch rate q of missile. (f) The actuator output δ_c . (g) The estimate of the upper bound of the interference norm D_1 . (h) The estimate of the upper bound of the interference norm D_3 . (i) The estimate of the parameter θ_1 . (j) The estimate of the parameter θ_3 . (k) The actor network weight norm. (l) The critic network weight norm.

χ). Figures 3(d), 4(d) and 5(d) display the normal acceleration n_L of the missile. Moreover, Figs 3(e), 4(e) and 5(e) show the pitch rate q of missile. The actuator outputs with validity faults and deviation faults are depicted in Figs 3(f), 4(f) and 5(f). The estimate of the upper bound of the interference norm D_1 , D_3 are given in Figs 3(g), (h), 4(g), (h), 5(g) and (h). The paradigms of the estimate of the parameter θ_1 and θ_3 are shown in Figs 3(i), (j), 4(i), (j), 5(i) and (j). The weight paradigms for actor-critic neural network are depicted in Figs 3(k), (l), 4(k), (l), 5(k) and (l). In conclusion, the results show that the interception strategy χ converges to zero and maintains accurate hit-kill interception even when the target possesses

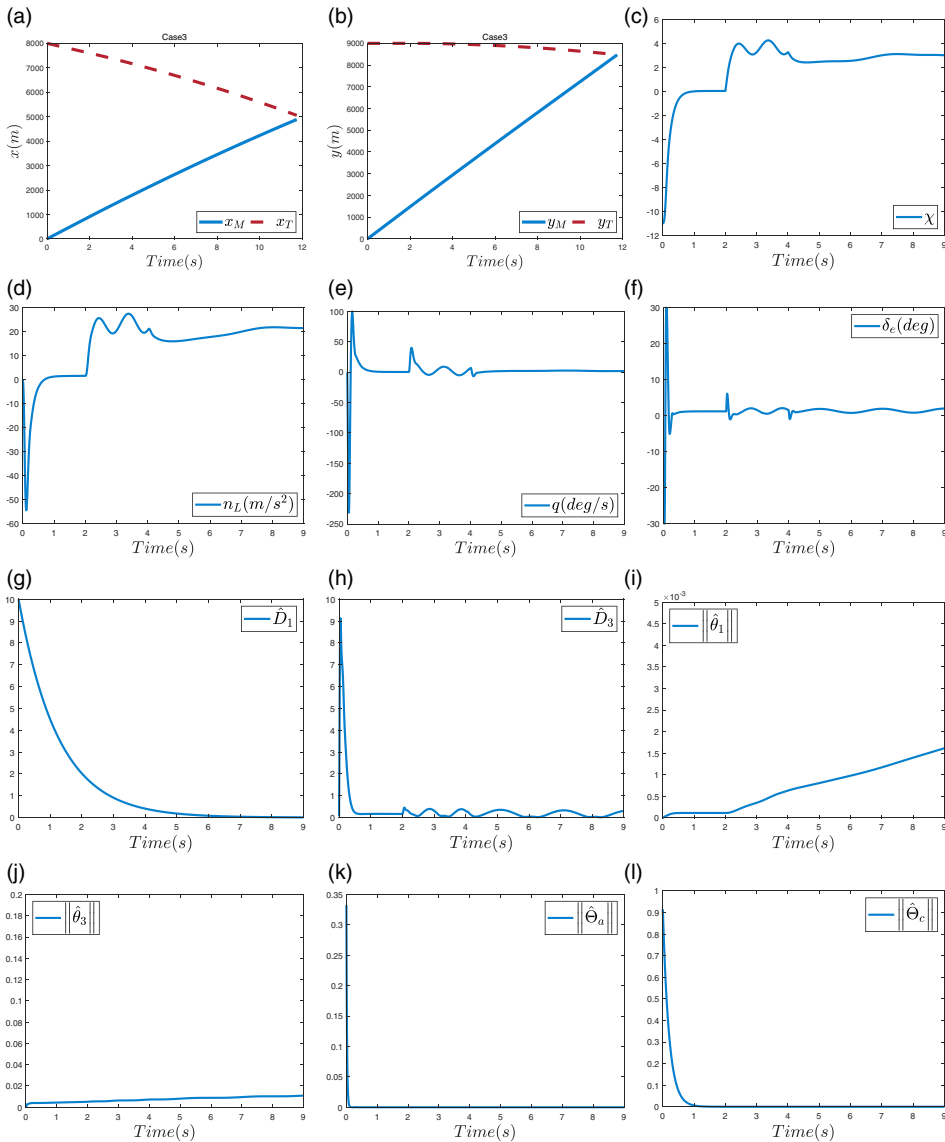


Figure 5. Simulation profiles for Case 3. (a) The x coordinates of missile and target. (b) The y coordinates of missile and target. (c) The guide variable χ . (d) The normal acceleration n_L of missile. (e) The pitch rate q of missile. (f) The actuator output δ_c . (g) The estimate of the upper bound of the interference norm D_1 . (h) The estimate of the upper bound of the interference norm D_3 . (i) The estimate of the parameter θ_1 . (j) The estimate of the parameter θ_3 . (k) The actor network weight norm. (l) The critic network weight norm.

time-varying acceleration and the missile has an actuator fault. As a result, the effectiveness of the proposed method can be verified.

At the same time, we compare the proposed control method of this paper with the backstepping fault-tolerant non-affine integrated guidance and control (BS-FTNAIGC) method, the adaptive boundary estimation fault-tolerant non-affine integrated guidance and control (ABE-FTNAIGC) method, and the radial basis function fault-tolerant non-affine integrated guidance and control (RBF-FTNAIGC) method. The initial conditions are as follows : the relative distance between projectile and target

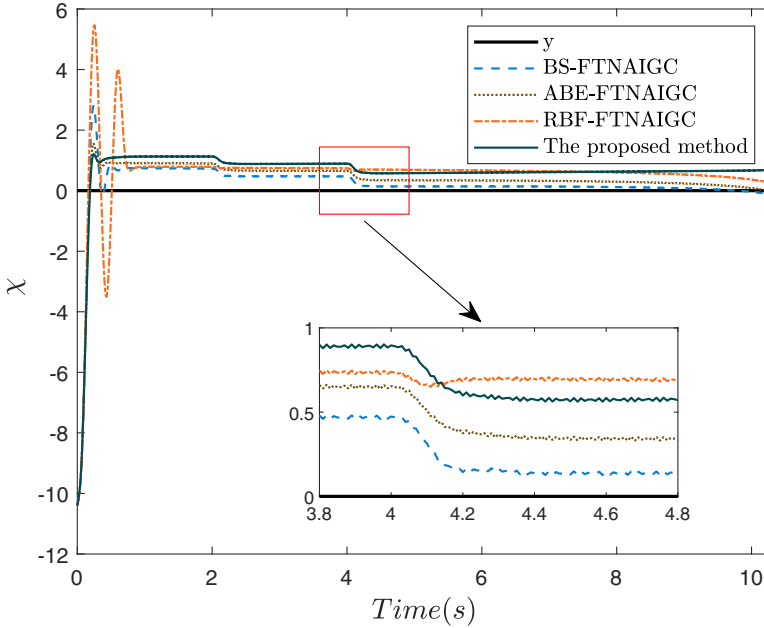


Figure 6. The guide variable χ .

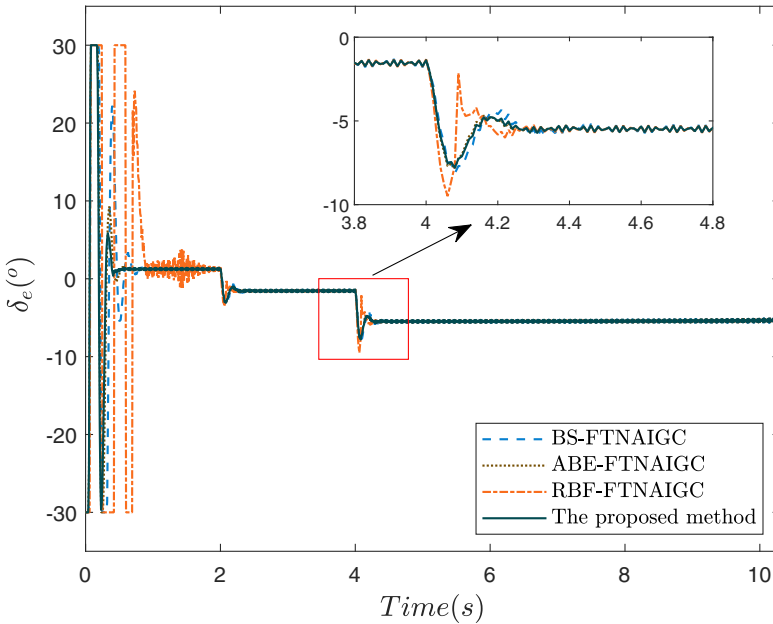


Figure 7. Actuator output δ_e .

along line of sight (LOS) $r(0) = 10,816.654m$, the angle between LOS and the horizontal reference line $\lambda = 0.588rad$, the target location $x_T = 9,000, y_T = 6,000$, the target acceleration $A_{T_r} = 5\sin(45*t)$, $A_{T_\lambda} = 10 + 4\sin(7.8/0.022*t)$. The actuator faults happen at $t > 2s$ with $\lambda_\delta = 0.8, d_\delta = 0.05$ and at $t > 4s$ with $\lambda_\delta = 0.6, d_\delta = 0.12$. Other initial conditions are the same as above. The specific comparison is as follows: Fig. 6 displays the system output in the four methods of the NAIGC system. The actuator fault outputs in the four methods of the NAIGC system are shown as Fig. 7. According to the simulation

results, it can be seen that the output of the controller and the control target of this paper are finally stable and convergent. At the same time, the overshoot and oscillation of the control method in this paper are smaller. Compared with other methods, the control method proposed in this paper can make the variables more quickly stable, and the steady-state error after stability is smaller. It can be seen that the actor-critic RBFNN has great advantages in the application of non-affine IGC systems.

5.0 Conclusion

In this paper, the NAIGC system is established for a class of STT missile with actuator failures, target acceleration variations and coupling multi-source uncertainties. The non-affine problem of the established model can be solved by the newly introduced integral expansion system. By introducing hyperbolic tangent function, RBFNN and reinforcement learning actor-critic neural network architecture, different adaptive laws and gradient descent update laws are constructed, which can reduce the deviation of actuator fault and target acceleration change, and effectively compensate the influence of multi-source uncertainty. Therefore, this paper not only designs a non-affine IGC model which is more suitable for practical application, but also proposes a new control method to apply reinforcement learning actor-critic to NAIGC, which can achieve accurate hit guidance. Finally, the effectiveness and superiority of the proposed method are verified by numerical simulation. In the future, we will study 3D IGC and add constraints.

Acknowledgements. This work was supported in part by the Foundation of China National Key Laboratory of Science and Technology on Test Physics & Numerical Mathematics (Grant Number: JP2022-800006000107-237), the Foundation of China National Key Laboratory of Science and Technology on Test Physics & Numerical Mathematics (Grant Number: 08-YY-2023-R11) and the National Natural Science Foundation of China (Grant Number: 62303378). Meanwhile, it was also supported by the Foundation of Shanghai Astronautics Science and Technology Innovation (Grant Number: SAST2022-114).

Competing interests. The authors declare none.

References

- [1] Guo, Z., Wang, J., Hu, G. and Guo, J. Research review on uncertainty observation techniques and control methods for aerospace vehicles, *Aerospace Technol.*, 2022, (5), pp 31–44. doi: [10.16338/j.issn.2097-0714.20220091](https://doi.org/10.16338/j.issn.2097-0714.20220091)
- [2] Wu, Y., Lu, X. and Wang, Z. Research on integrated design of aircraft spiral maneuver, guidance and control based on sliding mode control, *Beijing Ligong Daxue Xuebao/Trans. Beijing Inst. Technol.*, 2022, **42**, (5), pp 523–529. doi: [10.15918/j.tbit1001-0645.2021.089](https://doi.org/10.15918/j.tbit1001-0645.2021.089)
- [3] Wang, X., Zhang, X., Lin, P. and Li, W. Integrated strategy of penetration and attack based on optimal control, *Flight Dyn.*, 2022, **40**, (6), 51–60+71. doi: [10.13645/j.cnki.f.d.20220716.001](https://doi.org/10.13645/j.cnki.f.d.20220716.001)
- [4] Xu, M., Chen, G. and Wang, W. Aero-control integrated design for reusable launch vehicle based on feedback linearization, *Meas. Control Technol.*, 2018, **37**, (9), pp 88–91. doi: [10.19708/j.cjks.2018.09.021](https://doi.org/10.19708/j.cjks.2018.09.021)
- [5] Hu, C., Wei, Y. and Wang, X. Fixed-time integrated guidance and control for impact angle constrained interception with multiple uncertainties, *J. Projectiles Rockets Missiles Guidance*, 2023, **43**, (4), pp 98–104. doi: [10.15892/j.cnki.djzdx.2023.04.015](https://doi.org/10.15892/j.cnki.djzdx.2023.04.015)
- [6] Jiang, S., qing Tian, F., yan Sun, S. and ge Liang, W. Integrated guidance and control of guided projectile with multiple constraints based on fuzzy adaptive and dynamic surface, *Def. Technol.*, 2020 **16**, (6), pp 1130–1141. doi: [10.1016/j.dt.2019.12.003](https://doi.org/10.1016/j.dt.2019.12.003)
- [7] Zhao, K., Cao, D.Q. and Huang, W.H. Integrated guidance and control design for reentry warhead based on adrc, *Yuhang Xuebao/J. Astronaut.*, 2017, **38**, (10), pp 1068–1078. doi: [10.3873/j.issn.1000-1328.2017.10.007](https://doi.org/10.3873/j.issn.1000-1328.2017.10.007)
- [8] Wang, Z., Yuan, J., Pan, Y. and Wei, J. Neural network-based adaptive fault tolerant consensus control for a class of high order multiagent systems with input quantization and time-varying parameters, *Neurocomputing*, 2017, **266**, pp 315–324. <https://doi.org/10.1016/j.neucom.2017.05.043>
- [9] Wang, Z., Zhang, B. and Yuan, J. Decentralized adaptive fault tolerant control for a class of interconnected systems with nonlinear multisource disturbances, *J. Franklin Inst.*, 2018, **355**, (11), pp 4493–4514. doi: [10.1016/j.jfranklin.2017.10.038](https://doi.org/10.1016/j.jfranklin.2017.10.038)
- [10] Wang, Z. and Yuan, J. Fuzzy adaptive fault tolerant igr method for stt missiles with time-varying actuator faults and multisource uncertainties, *J. Franklin Inst.*, 2020, **357**, (1), pp 59–81. doi: [10.1016/j.jfranklin.2019.09.032](https://doi.org/10.1016/j.jfranklin.2019.09.032)
- [11] Najafi, A., Vu, M.T., Mobayen, S., Asad, J.H. and Fekih, A. Adaptive barrier fast terminal sliding mode actuator fault tolerant control approach for quadrotor uavs, *Mathematics*, 2022, **10**, (16), pp 1–22. doi: [10.3390/math10163009](https://doi.org/10.3390/math10163009)
- [12] Zhao, L., Zhao, F. and Che, W.W. Distributed adaptive fuzzy fault-tolerant control for multi-agent systems with node faults and denial-of-service attacks, *Inf. Sci.*, 2023, **631**, pp 385–395. doi: [10.1016/j.ins.2023.02.059](https://doi.org/10.1016/j.ins.2023.02.059)

- [13] Ashraffifar, A. and Jegarkandi, M.F. Adaptive fin failures tolerant integrated guidance and control based on backstepping sliding mode, *Trans. Inst. Meas. Control*, 2020, **42**, (10), pp 1823–1833. doi: [10.1177/0142331219897430](https://doi.org/10.1177/0142331219897430)
- [14] Zhao, D., Research on Integrated Guidance and Control Design of Hypersonic Flight Vehicle, Master's Thesis, Beijing Jiaotong University, No.3 Shangyuan Village, Haidian District, Beijing, China 2020.
- [15] Chen, K. Full state constrained stochastic adaptive integrated guidance and control for stt missiles with non-affine aerodynamic characteristics, *Inf. Sci.*, 2020, **529**, pp 42–58. doi: [10.1016/j.ins.2020.03.061](https://doi.org/10.1016/j.ins.2020.03.061)
- [16] Liu, Y.J., Li, S., Tong, S. and Chen, C.L., Adaptive reinforcement learning control based on neural approximation for non-linear discrete-time systems with unknown nonaffine dead-zone input, *IEEE Trans. Neural Networks Learn. Syst.*, 2019, **30**, (1), pp 295–305. doi: [10.1109/TNNLS.2018.2844165](https://doi.org/10.1109/TNNLS.2018.2844165)
- [17] Lopez, V.G. and Lewis, F.L. Dynamic multiobjective control for continuous-time systems using reinforcement learning, *IEEE Trans. Autom. Control*, 2019, **64**, (7), pp 2869–2874. doi: [10.1109/TAC.2018.2869462](https://doi.org/10.1109/TAC.2018.2869462)
- [18] Ruelens, F., Claessens, B.J., Quaiyum, S., De Schutter, B., Babuška, R. and Belmans, R. Reinforcement learning applied to an electric water heater: From theory to practice, *IEEE Trans. Smart Grid*, 2018, **9**, (4), pp 3792–3800. doi: [10.1109/TSG.2016.2640184](https://doi.org/10.1109/TSG.2016.2640184).
- [19] Xue, L., Sun, C., Wunsch, D., Zhou, Y. and Yu, F. An adaptive strategy via reinforcement learning for the prisoner's dilemma game, *IEEE/CAA J. Autom. Sinica*, 2018, **5**, (1), pp 301–310. doi: [10.1109/JAS.2017.7510466](https://doi.org/10.1109/JAS.2017.7510466)
- [20] Peng, Z., Hu, J., Shi, K., Luo, R., Huang, R., Ghosh, B.K. and Huang, J. A novel optimal bipartite consensus control scheme for unknown multi-agent systems via model-free reinforcement learning, *Appl. Math. Comput.*, 2020, **369**, p 124821. doi: [10.1016/j.amc.2019.124821](https://doi.org/10.1016/j.amc.2019.124821)
- [21] Yang, Y., Modares, H., Wunsch, D.C. and Yin, Y. Leader-follower output synchronization of linear heterogeneous systems with active leader using reinforcement learning, *IEEE Trans. Neural Networks and Learn. Syst.*, 2018, **29**, (6), pp 2139–2153. doi: [10.1109/TNNLS.2018.2803059](https://doi.org/10.1109/TNNLS.2018.2803059)
- [22] Fan, Q.Y., Yang, G.H. and Ye, D. Quantization-based adaptive actor-critic tracking control with tracking error constraints, *IEEE Trans. Neural Networks Learn. Syst.*, 2018, **29**, (4), pp 970–980. doi: [10.1109/TNNLS.2017.2651104](https://doi.org/10.1109/TNNLS.2017.2651104)
- [23] Hu, L., Li, R., Xue, T. and Liu, Y. Neuro-adaptive tracking control of a hypersonic flight vehicle with uncertainties using reinforcement synthesis, *Neurocomputing*, 2018, **285**, pp 141–153. doi: [10.1016/j.neucom.2018.01.031](https://doi.org/10.1016/j.neucom.2018.01.031)
- [24] Ouyang, Y., Dong, L., Wei, Y. and Sun, C. Neural network based tracking control for an elastic joint robot with input constraint via actor-critic design, *Neurocomputing*, 2020, **409**, pp 286–295. doi: [10.1016/j.neucom.2020.05.067](https://doi.org/10.1016/j.neucom.2020.05.067)
- [25] Liu, J., Shan, J., Rong, J. and Zheng, X. Incremental reinforcement learning flight control with adaptive learning rate, *J. Astronaut.*, 2022, **43**, (1), pp 111–121. doi: [10.3873/j.issn.1000-1328.2022.01.013](https://doi.org/10.3873/j.issn.1000-1328.2022.01.013)
- [26] Bohao, L., Xuman, A., Xiaofei, Y., Yunjie, W. and Guofei, L. A distributed reinforcement learning guidance method under impact angle constraints, *J. Astronaut.*, 2022, **43**, (8), pp 1061–1069. doi: [10.3873/j.issn.1000-1328.2022.08.008](https://doi.org/10.3873/j.issn.1000-1328.2022.08.008)
- [27] Pei, P., Shao-ming, H., Jiang, W. and De-fu, L. Integrated guidance and control for missile using deep reinforcement learning, *J. Astronaut.*, 2021, **42**, (10), pp 1293–1304. doi: [10.3873/j.issn.1000-1328.2021.10.010](https://doi.org/10.3873/j.issn.1000-1328.2021.10.010)
- [28] Song, J., Luo, Y., Zhao, M., Hu, Y. and Zhang, Y. Fault-tolerant integrated guidance and control design for hypersonic vehicle based on ppo, *Mathematics*, 2022, **10**, (18), pp 1–13. doi: [10.3390/math10183401](https://doi.org/10.3390/math10183401)
- [29] Wang, W., Xiong, S., Wang, S., Song, S. and Lai, C. Three dimensional impact angle constrained integrated guidance and control for missiles with input saturation and actuator failure, *Aerospace Sci. Technol.*, 2016, **53**, pp 169–187. doi: [10.1016/j.ast.2016.03.015](https://doi.org/10.1016/j.ast.2016.03.015)
- [30] Wang, Z. and Yuan, J. Full state constrained adaptive fuzzy control for stochastic nonlinear switched systems with input quantization, *IEEE Trans. Fuzzy Syst.*, 2020, **28**, (4), pp 645–657. doi: [10.1109/TFUZZ.2019.2912150](https://doi.org/10.1109/TFUZZ.2019.2912150)
- [31] Huang, J. Research on Command Filter Based Adaptive Control Algorithm For Nonlinear Systems with Full State Constraints, Master's Thesis, Yangzhou University, No. 88, University South Road, Yangzhou City, Jiangsu Province, China, 2023.
- [32] Xia, J., Lian, Y., Su, S.-F., Shen, H. and Chen, G. Observer-based event-triggered adaptive fuzzy control for unmeasured stochastic nonlinear systems with unknown control directions, *IEEE Trans. Cybern.*, 2022, **52**, (10), pp 10655–10666. doi: [10.1109/TCYB.2021.3069853](https://doi.org/10.1109/TCYB.2021.3069853)
- [33] He, W. and Dong, Y. Adaptive fuzzy neural network control for a constrained robot using impedance learning, *IEEE Trans. Neural Networks Learn. Syst.*, 2018, **29**, (4), pp 1174–1186. doi: [10.1109/TNNLS.2017.2665581](https://doi.org/10.1109/TNNLS.2017.2665581)
- [34] Wang, Z., Yuan, J., Pan, Y. and Che, D. Adaptive neural control for high order markovian jump nonlinear systems with unmodeled dynamics and dead zone inputs, *Neurocomputing*, 2017, **247**, pp 62–72. doi: [10.1016/j.neucom.2017.03.041](https://doi.org/10.1016/j.neucom.2017.03.041)
- [35] Yu, D., Long, J., Chen, C.L.P. and Wang, Z. Adaptive swarm control within saturated input based on nonlinear coupling degree, *IEEE Trans. Syst. Man Cybern. Syst.*, 2022, **52**, (8), pp 4900–4911. doi: [10.1109/TSMC.2021.3102587](https://doi.org/10.1109/TSMC.2021.3102587)